






The Cause of an Extremely Low Salinity Anomaly in the Bay of Bengal During 2012 Spring

Zhiyuan Li^{1,2} , Tao Lian^{2,3,4} , Jun Ying^{2,4}, Xiao-Hua Zhu^{2,3,4} , Fabrice Papa^{5,6} , Huawei Xie¹, and Yu Long² 

¹Key Laboratory for Technology in Rural Water Management of Zhejiang, Zhejiang University of Water Resources and Electric Power, Hangzhou, China, ²State Key Laboratory of Satellite Ocean Environment Dynamics, Second Institute of Oceanography, Ministry of Natural Resources, Hangzhou, China, ³School of Oceanography, Shanghai Jiao Tong University, Shanghai, China, ⁴Southern Marine Science and Engineering Guangdong Laboratory (Zhuhai), Zhuhai, China, ⁵LEGOS, Institut de Recherche pour le Développement, CNRS/IRD/CNES/Toulouse University, Toulouse, France, ⁶Indo-French Cell for Water Sciences, IRD-IISc Joint Laboratory, Indian Institute of Science, Bangalore, India

Key Points:

- An extremely low salinity anomaly was observed in the Bay of Bengal from various in situ and satellite observations in the spring of 2012
- Reversing circulation anomalies caused by a rare co-occurrence of positive Indian Ocean Dipole and La Niña in 2011 explain the extreme event
- The key process was the modulation of the seasonal monsoon by interannual processes, specifically the rare combination event 2011

Supporting Information:

Supporting Information may be found in the online version of this article.

Correspondence to:

X.-H. Zhu,
xhzhu@sio.org.cn

Citation:

Li, Z., Lian, T., Ying, J., Zhu, X.-H., Papa, F., Xie, H., & Long, Y. (2021). The cause of an extremely low salinity anomaly in the Bay of Bengal during 2012 spring. *Journal of Geophysical Research: Oceans*, 126, e2021JC017361. <https://doi.org/10.1029/2021JC017361>

Received 14 MAR 2021

Accepted 28 SEP 2021

Abstract An extremely low salinity anomaly was observed in the Bay of Bengal (BoB) by various in situ and satellite observations during 2012 spring and ranked as the strongest anomaly in the last two decades. By analyzing various observational and reanalysis datasets, we find that the reversing circulation anomalies caused by a rare co-occurrence of positive Indian Ocean Dipole (pIOD) and La Niña in 2011 were the main cause of this extreme event. In the fall of 2011, the pIOD favored an anticyclonic circulation anomaly flowing from the BoB into the equatorial Indian Ocean, whereas the La Niña event, which matured in the following winter, sharply reversed the circulation anomaly to a cyclonic pattern. As a result, these reversing circulation anomalies inhibited the southward freshwater transport along the two sides of the BoB and trapped substantial freshwater to the northern bay by the end of winter. Thereafter, the strong seasonal anticyclonic circulation transported this freshwater into the central and southern bay from the northeastern BoB coastal area, forming the extremely low salinity anomaly during 2012 spring. The key process in forming the extremely low salinity anomaly was the modulation of the seasonal monsoon by interannual processes, specifically the rare combination of pIOD and La Niña in 2011. Our results highlight the important role of the oceanic circulation in the sea surface salinity (SSS) variability in the BoB. This study provides some new perspectives on the SSS interannual variability in the BoB and the freshwater exchange between the BoB and Arabian Sea.

Plain Language Summary The Bay of Bengal (BoB) is a unique semienclosed basin in the tropical ocean that is characterized by a large amount of freshwater fluxes from rivers and a positive residual of precipitation minus evaporation. This freshwater is transported by large-scale circulation, causing strong seasonal variation in the sea surface salinity (SSS) in the BoB. Influenced by the Indian Ocean Dipole (IOD) and El Niño-Southern Oscillation, the SSS in the BoB also shows clear interannual variability. Uncommonly, an extremely low salinity anomaly was observed in the BoB from various observations during 2012 spring. The extreme anomaly was characterized by large-scale, long period and deep depth features and ranked as the lowest springtime SSS in the BoB in the last two decades. The analysis shows that anomalous freshwater transport in the BoB played a major role, while the local freshwater fluxes played a minor role. The key process was the seasonal freshwater transport modulated by reversing circulation anomalies in the BoB and eastern equatorial Indian Ocean during a rare co-occurrence of positive IOD and La Niña in 2011. This work has implications for the SSS interannual variability in the BoB and freshwater exchange between the BoB and the Arabian Sea.

1. Introduction

The Bay of Bengal (BoB) is a semienclosed basin in the northern Indian Ocean with a feature of a distinct region of low sea surface salinity (SSS) (Figure 1a). The low SSS distribution is maintained by a positive residual of precipitation minus evaporation (P-E) and excessive runoff (R) from several major rivers during the summer monsoon (Figures 1b and 1c) (Han et al., 2001; Papa et al., 2010, 2012; Sengupta et al., 2006; Zhou & Murtugudde, 2014). For example, the Ganges-Brahmaputra (GB) and Irrawaddy rivers are among one of the world's largest rivers and discharge substantial continental freshwater into the BoB

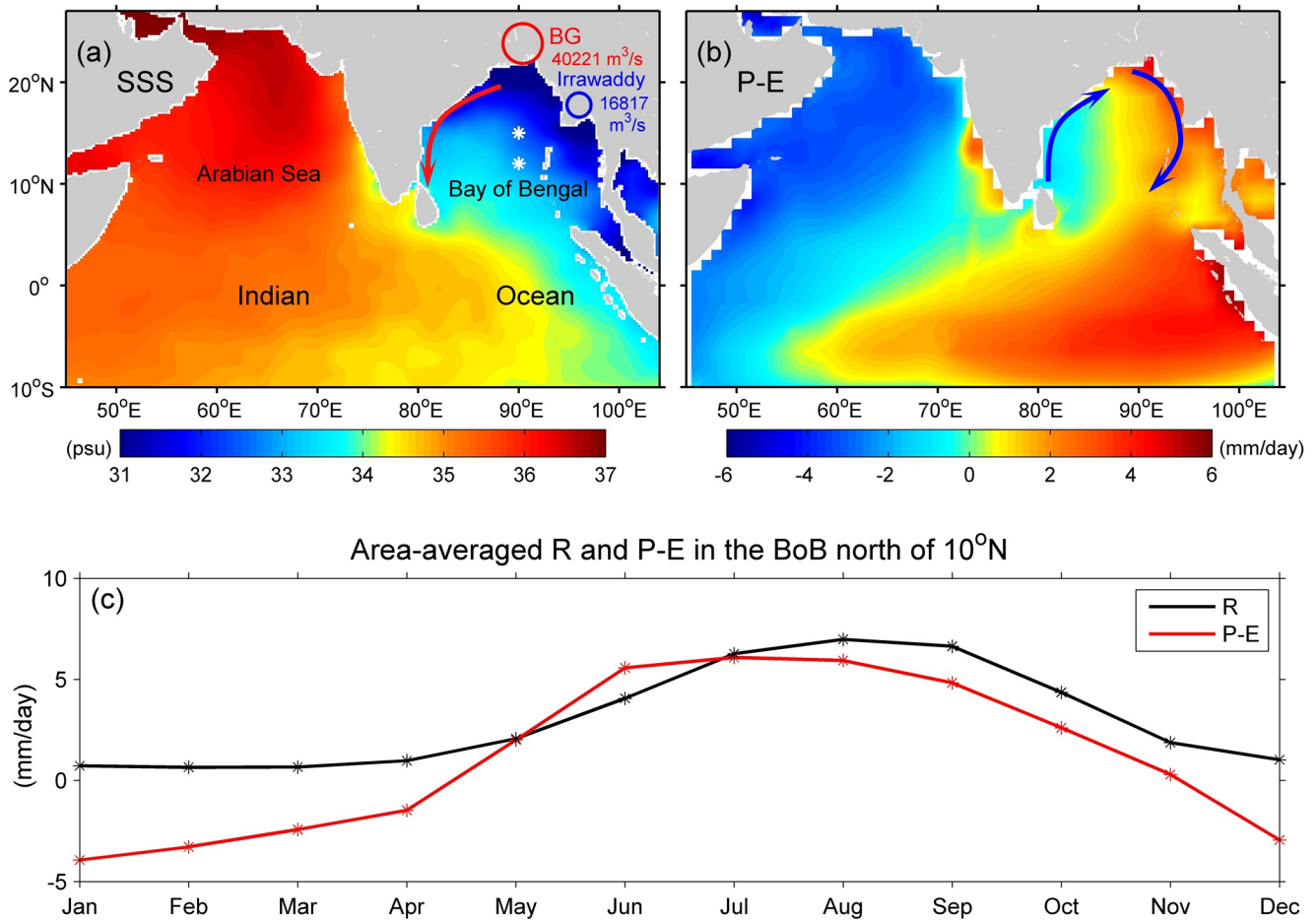


Figure 1. Annual mean WOA18 SSS (a) and P-E (b) based on the GPCP precipitation and OAF flux evaporation from 1979 to 2018. The white asterisks represent the RAMA buoys at stations B15 (15°N, 90°E) and B12 (12°N, 90°E) in the BoB. The red arrow denotes the southward EICC during fall to winter, and the blue arrows indicate the anticyclonic circulation in the BoB during spring. The circles indicate the locations of the GB and Irrawaddy rivers and their sizes are proportional to the magnitudes of the annual mean discharge. (c) Climatological monthly evolution of R (black) from BG and Irrawaddy rivers and P-E (red) in the BoB north of 10°N (integrated over the ocean only).

(Figure 1a). The freshwater causes strong near-surface stratification and a thick barrier layer in the BoB, thus playing an important role in local mixed layer thermodynamics and air-sea interactions (Girishkumar et al., 2013, 2017; Li, Han, Ravichandran, et al., 2017; Li, Han, Wang, et al., 2017; Sprintall & Tomczak, 1992; Thadathil et al., 2007, 2016; Vinayachandran et al., 2002).

The freshwater in the BoB is transported by large-scale circulation, leading to strong seasonal SSS variations. Previous studies proposed two pathways of the freshwater: one pathway is the East Indian Coastal Current (EICC), which transports freshwater along the eastern Indian coast during the fall to winter (Akhil et al., 2014; Chaitanya et al., 2014; Fournier et al., 2017; Murty et al., 1992; Sengupta et al., 2016; Shetye et al., 1996), and the other is the anticyclonic gyre, which transports freshwater from the northeastern BoB into the Arabian Sea (AS) during spring (Han & McCreary, 2001; Jensen, 2001, 2007). It is worth noting that the second freshwater pathway was found only based on model simulation, and evidence from in situ observations is still missing.

The SSS in the BoB also exhibits strong interannual variability which is primarily associated with the Indian Ocean Dipole (IOD) and the El Niño-Southern Oscillation (ENSO; Du & Zhang, 2015; Grunseich et al., 2011; J. Li et al., 2016; Pant et al., 2015; Saji et al., 1999; Sherin et al., 2018; Subrahmanyam et al., 2011, 2018; Thompson et al., 2006; Webster et al., 1999). Moreover, IOD and ENSO can co-occur with each other (Saji & Yamagata, 2003; Stuecker et al., 2017). For example, positive IOD (pIOD) can co-occur

with El Niño and negative IOD (nIOD) can co-occur with La Niña (Cai et al., 2009; Gnanaseelan et al., 2012; Hong et al., 2008). During pIOD years, an anticyclonic circulation anomaly is formed in the BoB and transports freshwater from the eastern bay into the equatorial Indian Ocean (EIO; Du et al., 2020; Grunseich et al., 2011; Lian et al., 2014; Subrahmanyam et al., 2011; Thompson et al., 2006; Zhang et al., 2018). During La Niña years, the anomalies in the BoB and EIO are opposite to those during pIOD events (Gnanaseelan et al., 2012; Stuecker et al., 2017).

Uncommonly, an extremely low salinity anomaly was observed in the BoB in the spring of 2012. However, the spatial characteristics and reasons for its formation are not well studied, and the associated processes are still unclear. In this study, we explore the underlying dynamics of this event using various in situ and satellite data. We show for the first time that this extreme event was associated with the reversing circulation anomalies caused by a rare co-occurrence of pIOD and La Niña in 2011. The rest of the manuscript is organized as follows. The data and method used in this study are described in Section 2. The characteristics and formation mechanisms of the extremely low salinity anomaly in the spring of 2012 are investigated in Section 3. A discussion is provided in Section 4, and a summary is provided in Section 5.

2. Data and Method

2.1. Salinity Data

Daily salinity, temperature and potential density data measured by the Research Moored Array for African-Asian-Australian Monsoon Analysis and Prediction (RAMA) moored buoys (McPhaden et al., 2009) at 15°N, 90°E (B15) and 12°N, 90°E (B12) in the northern BoB are used. The RAMA data are provided by the Global Tropical Moored Buoy Array Project Office of the National Oceanic and Atmosphere Administration and the Pacific Marine Environmental Laboratory (<https://www.pmel.noaa.gov/>). The original data are vertically linearly interpolated into 1 m intervals and then smoothed with a 10-day running mean for analysis.

We use the global, 1° × 1° monthly salinity gridded Argo dataset from the Grid Point Value of the Monthly Objective Analysis using Argo float data (Hosoda et al., 2008), which are provided by the Japan Agency for Marine-Earth Science and Technology (JAMSTEC) (<http://www.jamstec.go.jp>). This Argo product combines data from Argo floats, Triangle Trans-Ocean Buoy Network and available conductivity-temperature-depth casts. The Argo dataset has a horizontal resolution of 1° × 1° at each standard pressure level, and the data are available from January 2001 to December 2018. We nominally consider the salinity at 10 m (first level) as that from the sea surface.

In June 2011, NASA launched the Aquarius/SAC-D mission with the primary goal of measuring SSS on a global scale from space. Based on the 1° × 1° Aquarius SSS data distributed by NASA's Physical Oceanography Distributed Active Archive Center, the Asia-Pacific Data-Research Center of the International Pacific Research Center produced an optimal interpolation of SSS (OISSS) with a resolution of 0.5° × 0.5° (Mel-nichenko et al., 2014, 2015) (<http://apdrc.soest.hawaii.edu>). The OISSS data are available from August 27, 2011 to May 28, 2015 on a weekly scale and from September 2011 to May 2015 on a monthly scale.

The L3 V5.0 Soil Moisture Active Passive (SMAP) SSS produced by NASA's Jet Propulsion Laboratory (Fore et al., 2020) is used. The SMAP SSS data have a spatial resolution of 0.25° and are available from April 2015 to present. The data can be downloaded from the Asia-Pacific Data-Research Center of the International Pacific Research Center at the University of Hawaii (<http://apdrc.soest.hawaii.edu>).

We also use the climatological monthly World Ocean Atlas 2018 (WOA18) objective analyzed salinity field. The WOA18 data have a spatial resolution of 0.25° and are available at the National Centers for Environmental Information.

2.2. Altimeter and Wind Data

We use the global, 0.25° × 0.25° sea surface height (SSH) and reanalysis surface current for 1993–2018 from the Copernicus Marine and Environment Monitoring Service (CMEMS, <http://marine.copernicus.eu/>). The CMEMS global gridded Level-4 data are produced using measurements from all available satellite altimeters. The SSH is obtained by removing the mean dynamic topography from the absolute dynamic

topography. We use the monthly surface winds during 1993–2018 from the cross-calibrated multiplatform (CCMP) version 2.0 dataset (Atlas et al., 2011; Wentz et al., 2015). The anomalies are obtained by subtracting the monthly climatology from the data.

2.3. IOD and ENSO Indices

The IOD is characterized by the dipole mode index (DMI), which is defined as the difference of area-averaged sea surface temperature anomaly (SSTA) between the western (50°E–70°E, 10°S–10°N) and eastern (90°E–110°E, 10°S–0°) tropical Indian Ocean (Saji et al., 1999). The ENSO is characterized by the Oceanic Niño Index (ONI), which is defined as the area-averaged SSTA in the Niño 3.4 region. The DMI and ONI indexes are provided by the JAMESTEC and the National Oceanic and Atmospheric Administration Climate Prediction Center (NOAA-CPC), respectively.

2.4. Freshwater Fluxes Data

Papa et al. (2010, 2012) used altimetry derived river discharge, based on empirical regression curves between altimetry measured river water height and observed river discharge, to retrieve variations in the GB and Irrawaddy river freshwater fluxes into the BoB. We use the updated satellite-derived monthly river discharge products, now available from 1993 to 2020 for the GB and from 1993 to 2016 for the Irrawaddy (Papa et al., 2012). We use the 1° × 1° gridded monthly Objectively Analyzed Air-sea Fluxes (OAFflux) for evaporation (Yu & Weller, 2007) and the 2.5° × 2.5° gridded monthly Global Precipitation Climatology Project (GPCP) version 2.3 dataset for precipitation (Adler et al., 2003; Huffman et al., 2009) to build a monthly P-E product covering 1979–2018. We use linear interpolation to regrid the 2.5° × 2.5° GPCP data onto the 1° × 1° grid of the OAFflux data.

2.5. Mixed Layer Salt Budget

A salt budget is estimated in the BoB in order to determine the dominant processes responsible for the salinity variability in the mixed layer. The mixed layer salt budget is estimated using the following formula according to R. Rao and Sivakumar (2003) and Pant et al. (2015):

$$\frac{\partial S}{\partial t} = \frac{(E - P)}{h} S - \left[u \frac{\partial S}{\partial x} + v \frac{\partial S}{\partial y} \right] + \text{Re}s \quad (1)$$

(a) (b) (c) (d)

The terms of Equation 1 represent (a) salinity tendency, (b) local freshwater fluxes due to P-E, (c) horizontal advection, and (d) residual, where h is the mixed layer depth (MLD) and S and $\vec{u} = (u, v)$ are the salinity and horizontal velocity vertically averaged in the mixed layer.

To calculate these terms in Equation 1, we use the monthly Ocean ReAnalysis System 5 (ORAS5) products (including the salinity, MLD, horizontal velocity) from the European Center for Medium-Range Weather Forecasts (Zuo et al., 2019). ORAS5 has a spatial resolution of 0.25° × 0.25° and 75 layers vertically. A climatological state is built by using the ORAS5 products from 1979 to 2018.

2.6. SSS Product Intercomparison/Validation

To validate the accuracy of the SSS data, we make a comparison between the Argo, Aquarius, SMAP and WOA18 SSS. We linearly interpolate the Aquarius OISSS to the grid of the SMAP SSS to build a combination of satellite-based products from 2011 to 2018 (Figure 2b). The Argo, WOA18 and combination of Aquarius and SMAP dataset show similar spatial distributions: freshwater in the BoB, salty water in the AS and tongue-shaped salty water extending from the southern AS to the eastern EIO. To quantify the comparison, two boxes are selected in the BoB (box 1, 6°N–23°N, 79°E–99°E) and central EIO (box 2, 2.5°S–2.5°N, 70°E–90°E). The Argo area-averaged SSS in the two boxes compares well with the Aquarius and SMAP data. In box 1 (Figure 2c), the correlation coefficient between the Argo SSS and Aquarius OISSS is 0.91, and the root mean square difference (RMSD) is 0.16 psu. The correlation coefficient between the Argo SSS and

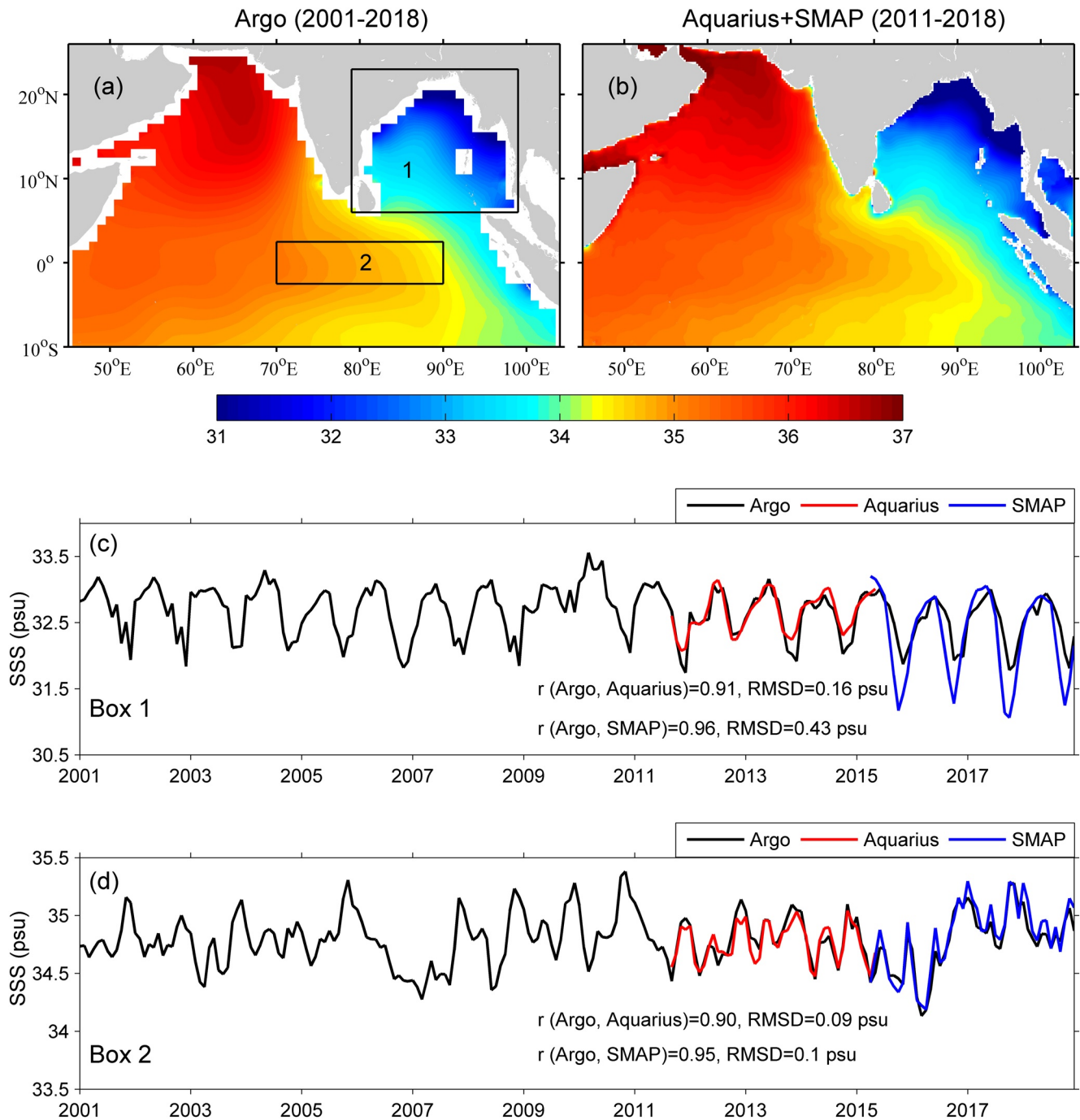


Figure 2. Annual mean SSS (psu) from Argo (a) and (b) combination of Aquarius and SMAP data. Comparisons between the time series of the Argo (black), Aquarius (red) and SMAP (blue) area-averaged SSS in box 1 (c) and box 2 (d). The correlation coefficients and RMSDs between the two time series are estimated for the period both data are available.

SMAP SSS is 0.96, and the RMSD is 0.43 psu. The relatively larger RMSD between the Argo SSS and SMAP SSS is because the Argo data are unavailable in coastal regions where the SMAP SSS is very low. In box 2 (Figure 2d), the correlation coefficient between the Argo SSS and Aquarius OISSS is 0.90, and the RMSD is 0.09 psu. The correlation coefficient between the Argo SSS and SMAP SSS is 0.95, and the RMSD is 0.1 psu. Overall, these comparisons indicate good agreement between the Argo SSS and other datasets.

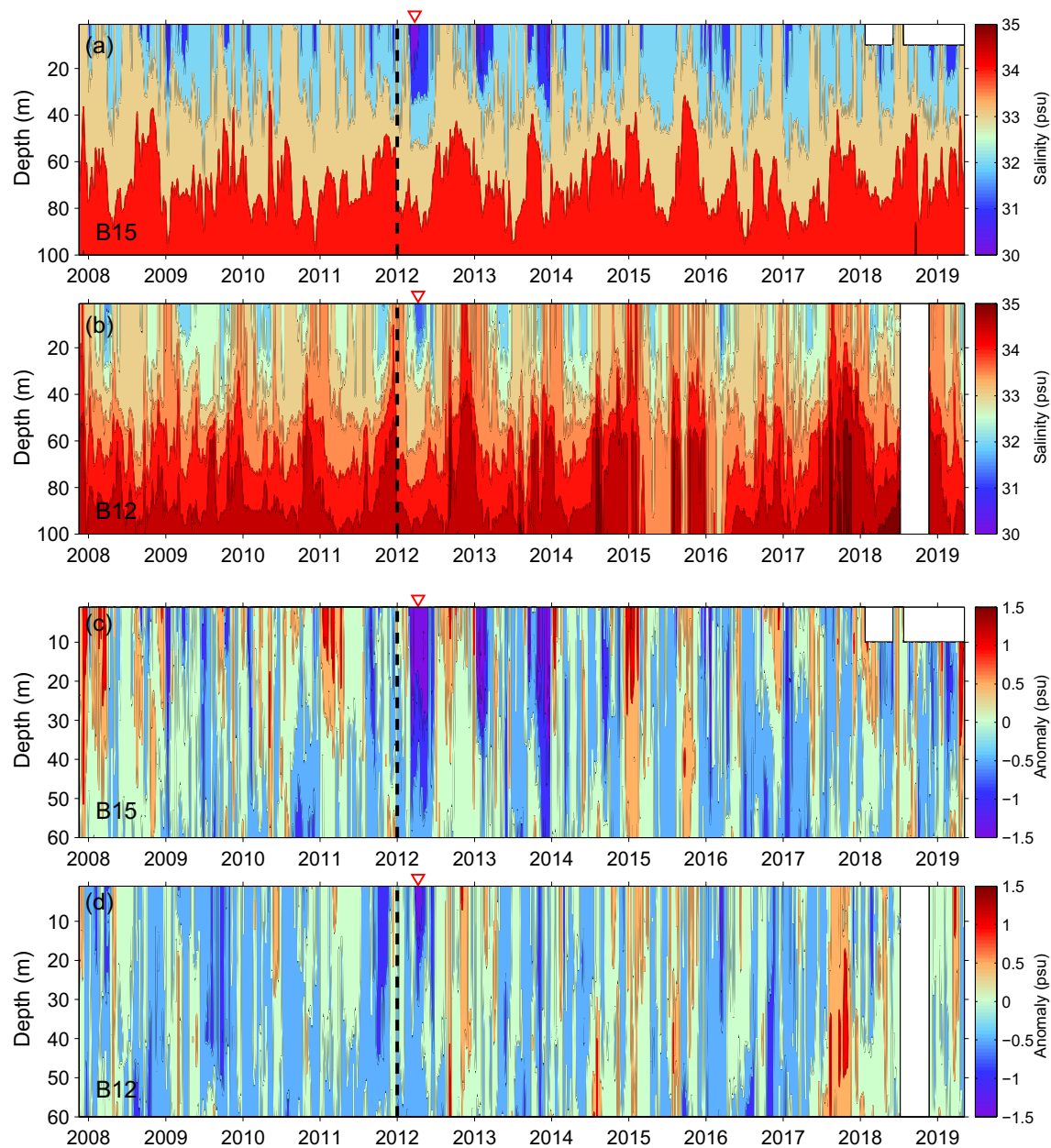


Figure 3. 10-day smoothed daily salinity and the anomaly measured by the RAMA buoys at stations B15 (a, c) and B12 (b, d). The black dashed line indicates the year 2012 and the red triangle highlights the extremely low salinity anomaly in the spring of 2012.

3. Results

3.1. An Extremely Low Salinity Anomaly During 2012 Spring

3.1.1. RAMA Buoy Observations

Figure 3 shows the 10-day smoothed daily salinity and the anomaly measured by the RAMA buoys at stations B15 (15°N, 90°E) and B12 (12°N, 90°E) since 2007. From an overall view, the RAMA buoy salinity is much lower at station B15 than station B12. At station B15, frequent low salinity events were observed during the whole observational period (Figure 3a). Most of these low salinity events occurred during summer to winter and were attributed to river freshwater modulated by the basin-scale circulation and mesoscale eddies (Fournier et al., 2017; Z. Li et al., 2021; Parampil et al., 2010; S. Rao et al., 2011; Sengupta et al., 2016; Sree Lekha et al., 2018; Suneel et al., 2020). For example, two significant low salinity events were recognized

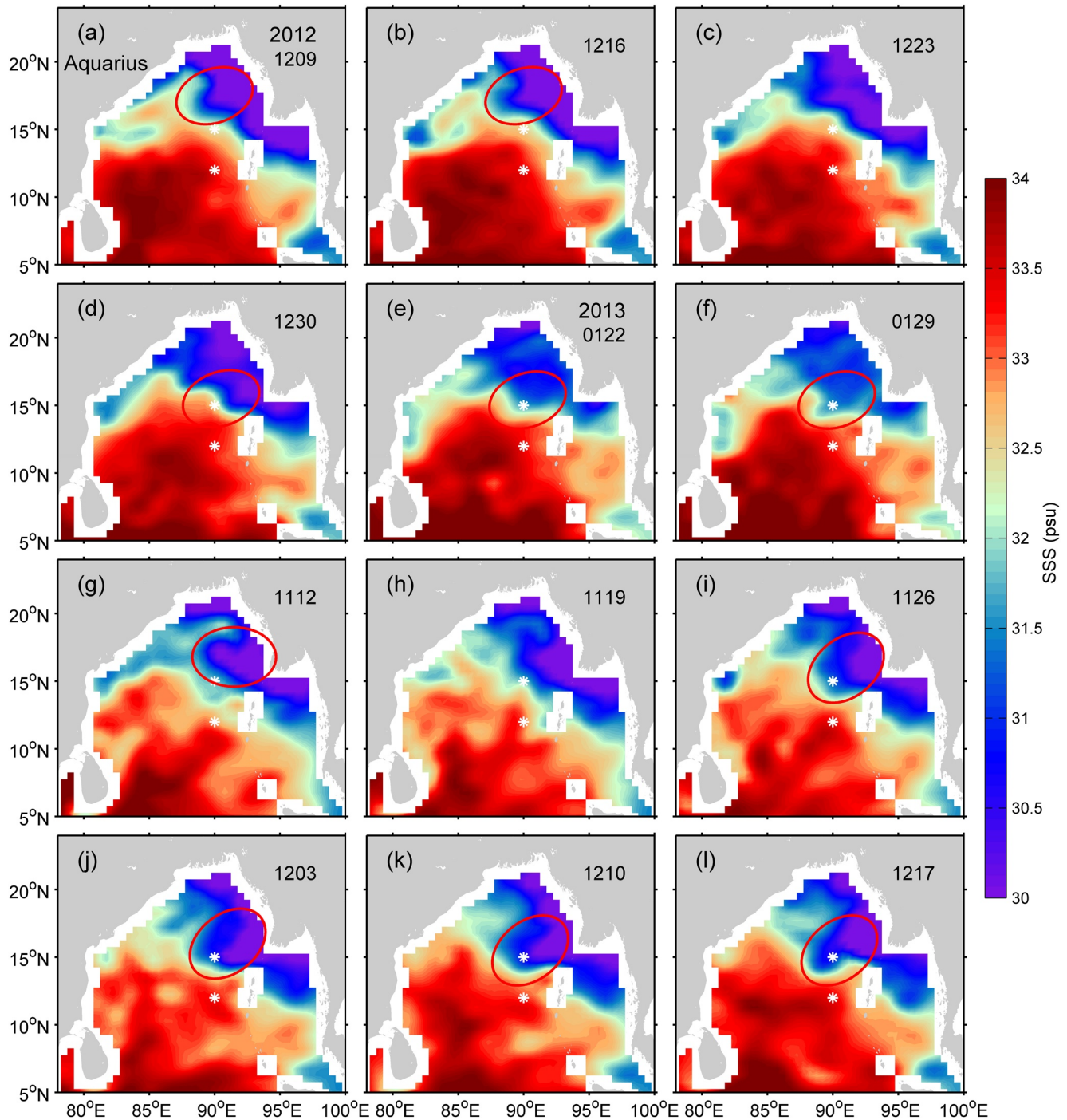


Figure 4. Snapshots of weekly Aquarius OISSS during the early and late winter of 2013. The white asterisks indicate the RAMA buoys at stations B15 and B12, and the red ellipses highlight the freshwater plumes extending offshore from the eastern BoB coast. The numbers in the upper right of the panels indicate the date from December 9, 2012 to January 29, 2012 (a–f) and (g–l) from November 12, 2013 to December 17, 2013.

in the early and late winter of 2013. It is confirmed from the snapshots of weekly Aquarius OISSS that these two low salinity events during 2013 winter were directly related to freshwater plumes extending offshore from the eastern BoB coast (Figure 4). The Aquarius OISSS maps show that the fronts of the freshwater plume reached the station B15 and caused a sharp decrease in SSS there.

Figures 3c and 3d show the salinity anomaly measured by the RAMA buoys at the two locations. In particular, an extremely low salinity anomaly was clearly identified in the spring of 2012 at both stations, especially the station B15. The extremely low salinity anomaly has a period of 3 months and a depth of approximately 60 m. Compared with the low salinity events that frequently occur during summer to winter, such an extremely low salinity anomaly during spring is uncommon (Figures 3a and 3c). However, this extremely low salinity anomaly is poorly reported, although it is the most significant anomaly throughout the whole observational period (Figures 3c and 3d). In the following, we use the Argo SSS and Aquarius OISSS data to further characterize the spatial pattern of this extremely low salinity anomaly in the spring of 2012.

3.1.2. Spatial Pattern

The spatial distribution of the extremely low salinity anomaly is shown in Figure 5. The Argo data show a low spring SSS throughout the whole BoB in 2012, with the lowest center at the east of the station B15 (Figure 5a). The spring SSSA shows that significant negative values (<-0.5 psu) can even reach south of the station B12 (Figure 5b). The maximum negative SSSA reached -1.0 psu and spanned more than 60 m in depth (Figures 5b and 5c). Interestingly, the salinity anomaly even reached 100 m in depth near 80°E (Figure 5c). The Aquarius OISSS shows similar features as the Argo SSS, confirming the low spring SSS in the BoB in 2012 (Figures 5c and 5d). The time series of the spring SSSA averaged over the northeastern BoB (red box in Figure 5b) confirms that the extremely low salinity anomaly in 2012 was ranked as the lowest springtime SSS in the last two decades (Figure 5f). Such a long time, large-scale, and deep salinity anomaly implies that a large-scale circulation anomaly may have contributed to the formation of this extremely low salinity anomaly.

3.2. A Rare Co-Occurrence of pIOD and La Niña in 2011

3.2.1. Composite Analysis

As mentioned above, the SSS interannual variability in the BoB is primarily associated with the IOD and ENSO (Akhil et al., 2016; Fournier et al., 2017; Grunseich et al., 2011; Pant et al., 2015; Thompson et al., 2006; Vinayachandran & Nanjundiah, 2009). Figures 6a and 6b show composites of the SSS and surface wind anomalies during fall (September–November, SON) in pIOD and La Niña years, respectively. In pIOD years, a strong easterly wind anomaly is noted in the EIO, which causes upwelling Kelvin waves propagating from the eastern EIO into the BoB and forms an anticyclonic circulation anomaly in the bay. Therefore, a negative SSSA is identified in the northern BoB that extends from the eastern bay into the EIO. This negative SSSA pattern reflects an anticyclonic freshwater transport from the BoB into the EIO. In La Niña years, the overall patterns of these variable anomalies are comparable in magnitude but opposite in sign with those in pIOD years (Figure 6b). Figures 6c and 6d show composites of the spring SSSA in the BoB after a pIOD and La Niña year. It clearly shows that the spring SSSA in the BoB in 2012 (Figure 5b) was much stronger than those in Figures 6c and 6d. This indicates that the SSSA in the BoB during the fall to winter of 2011 was different from those in normal pIOD and La Niña years.

3.2.2. Surface Wind, SSH and SSS Anomalies in 2011

Figure 7a shows the evolution of the DMI and ONI indexes in 2010–2011. Following a strong nIOD 2010, a pIOD developed in April–May of 2011, peaked in August–September and then quickly attenuated after October of 2011. A strong La Niña event occurred in mid-2010 and persisted until the early spring of 2012. Thus, a rare co-occurrence of pIOD and La Niña was identified in 2011 (Figure 7a). The scatterplots of the DMI and ONI indexes indicate that such a co-occurrence of pIOD and La Niña in 2011 was rare in the last four decades (Figure 7c). Another case of co-occurrence of pIOD and La Niña was found in 2007 (Figure 7c), as shown by Behera et al. (2008) and Cai et al. (2009). However, the two cases differ in terms of the IOD variability: the pIOD 2011 followed a nIOD 2010 (Figure 7a), while the pIOD 2007 was a consecutive event after a pIOD 2006 (Figure 7b). As a result, the circulation anomalies during the combination event 2007 were different from those during the combination event 2011, which will be shown in the discussion part.

Although the pIOD and La Niña worked against each other in changing the SSS in the BoB, the peak phase of the pIOD led the La Niña by about 2 months in 2011 (Figure 7a). Figure 8 shows the monthly SSHA in the BoB and eastern EIO from August 2011 to January 2012. The circulation anomaly (associated with

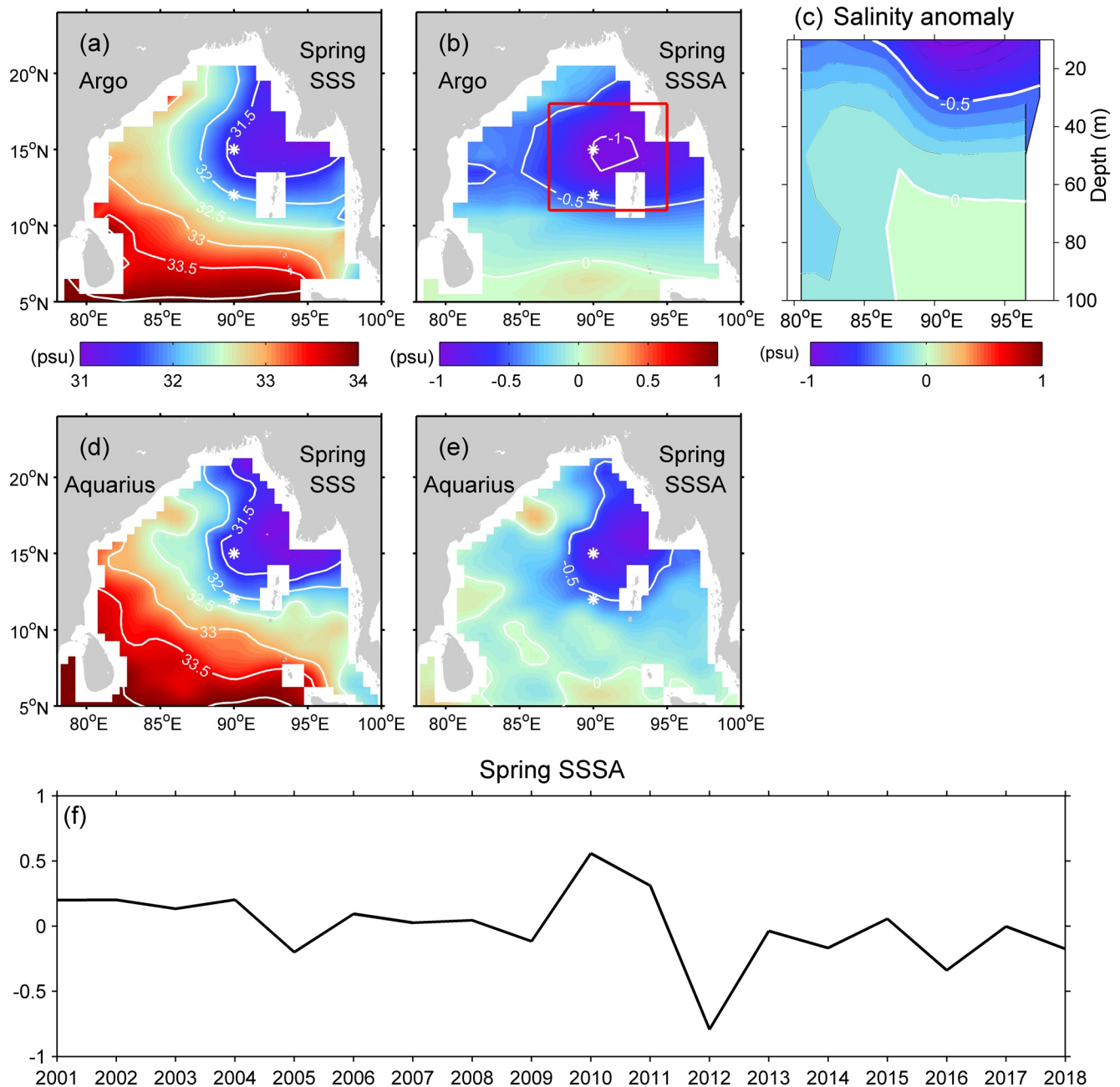


Figure 5. (a–c) Extremely low salinity anomaly in the spring of 2012 based on the Argo data (a–c) for SSS (a), SSSA (b) and (c) salinity anomaly along section 15°N in the BoB. The white asterisks indicate the RAMA buoys at stations B15 and B12, and the red box (11°N–18°N, 87°E–95°E) highlights the area with the maximum negative SSSA. (d–e) Same as a–b but for Aquarius data. (f) Time series of Argo spring SSSA averaged over the box in the northeastern BoB.

the SSHA) can be divided into three stages: during August–September, it showed an anticyclonic pattern flowing from the BoB into the eastern EIO (Figures 8a and 8b). These features are consistent with the circulation anomaly during the mature phase of normal pIOD years (Du et al., 2020; Gnanaseelan et al., 2012; Thompson et al., 2006). From October–November, the anticyclonic circulation anomaly was still present in the BoB. However, the current anomaly in the eastern EIO weakened significantly (Figures 8c and 8d). These features reflect the influences of the mature La Niña on the circulation anomaly in the eastern EIO. From December 2011 to January 2012, the anticyclonic circulation anomaly reversed to a cyclonic pattern flowing from the eastern EIO into the BoB (Figures 8e and 8f). These features correspond to the circulation anomaly during the mature phase in La Niña years (Gnanaseelan et al., 2012; Hong et al., 2008), reflecting

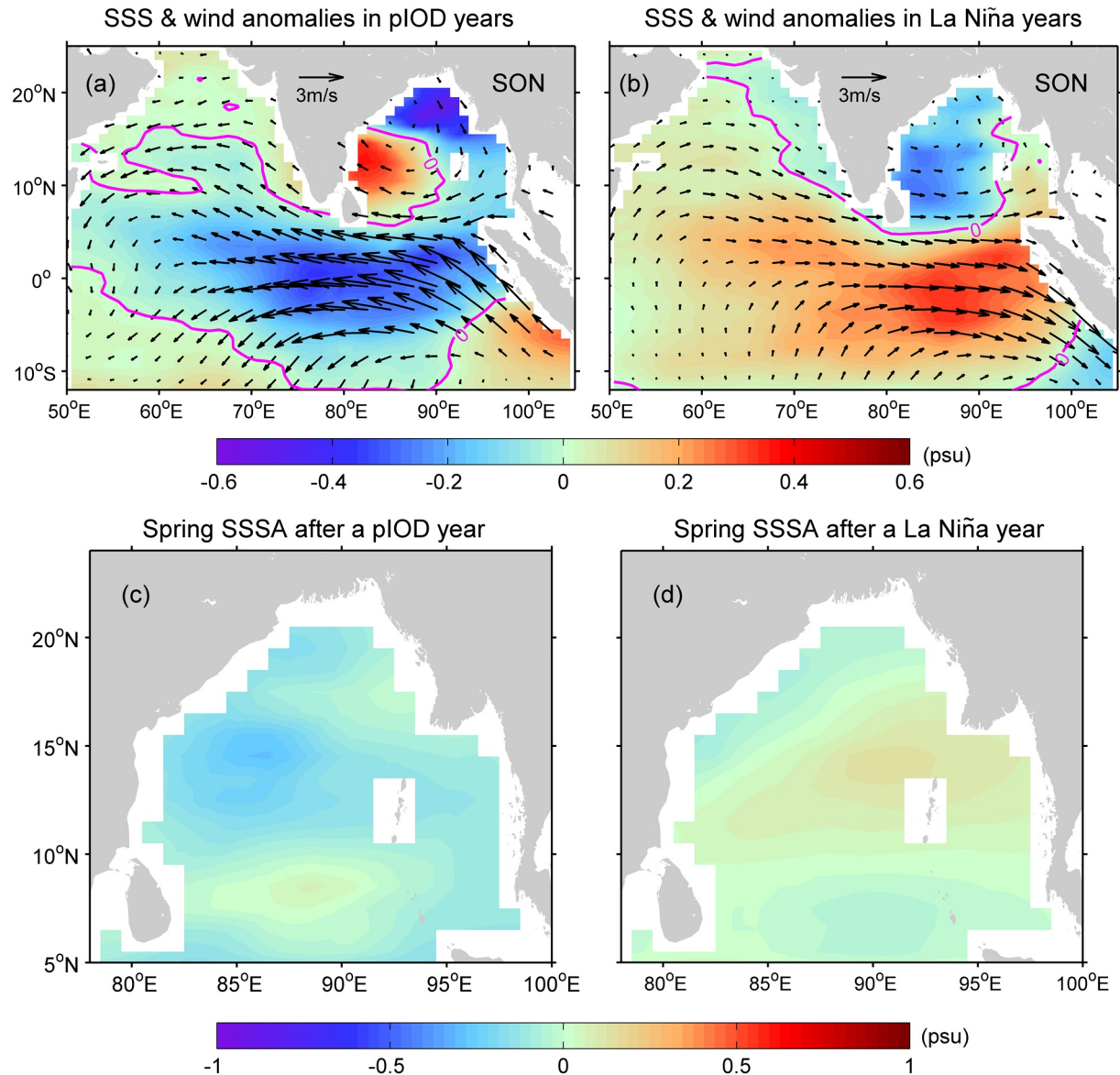


Figure 6. Composites of the SON CCMP surface wind (vector) and Argo SSS (color) anomalies in pIOD (a) and (b) La Niña years, and of the spring SSSA in the BoB after a pIOD (c) and (d) La Niña year. In the composite analysis, the pIOD (La Niña) year indicates a single pIOD (La Niña) event or combination of pIOD and El Niño (nIOD and La Niña). Thus, the pIOD years are 1994, 1997, 2006, 2012 and 2015 according to the Australian government Bureau of Meteorology, and the La Niña years are 1995, 1998, 1999, 2000, 2005, 2010, 2016 and 2017 according to the NOAA-CPC.

the dominant role of La Niña during this period. These reversing circulation anomalies in the BoB and eastern EIO reflect the alternating roles of pIOD and La Niña during the fall to winter in 2011.

We further examine the influences of these reversing circulation anomalies on the SSS variability in the BoB. Figure 9 presents the circulation, SSS and surface wind anomalies during the fall to winter in 2011. The fall season is from August to October, when the pIOD is the maximum. In the fall of 2011, the wind and circulation anomalies showed a wind-driven effect: a strong easterly wind anomaly generated upwelling Kelvin waves in the eastern EIO (Chen et al., 2015, 2016; Huang et al., 2021), which propagated into the BoB and formed an anticyclonic circulation anomaly pattern in the bay (Figure 9a). Thus, the anticyclonic circulation anomaly transported freshwater from the BoB into the eastern EIO. Then, the freshwater was further transported to the central EIO by the easterly jet anomaly there (Figure 9c). These features are consistent

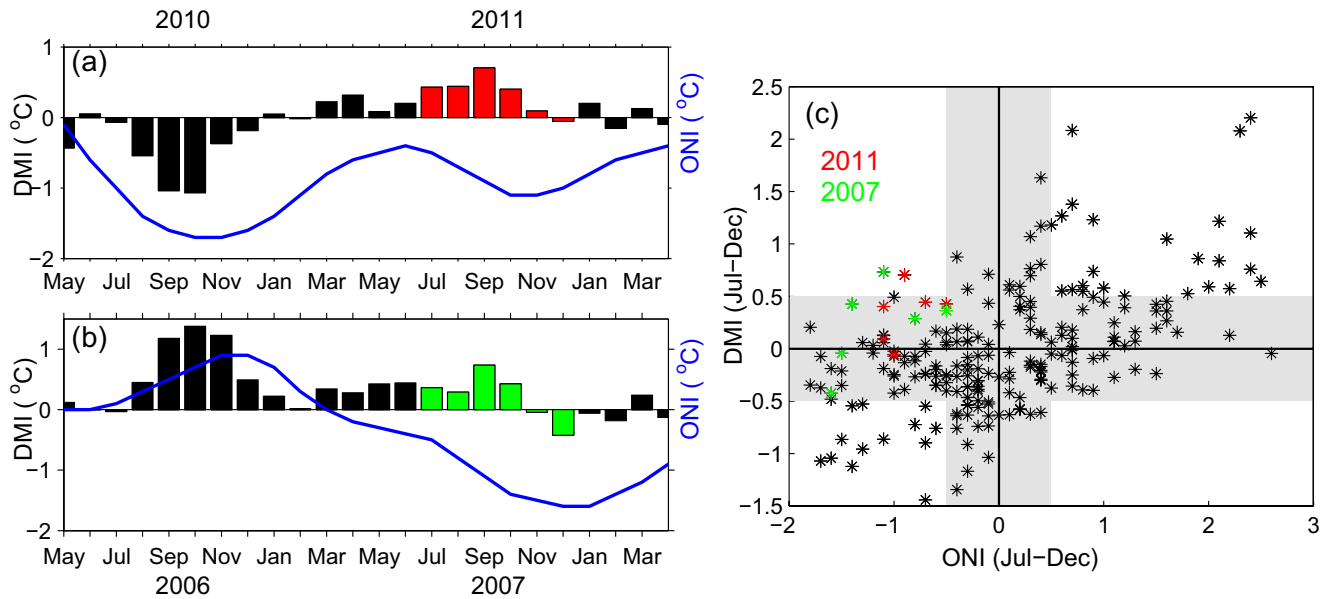


Figure 7. Evolution of the DMI (bar) and ONI (blue line) indexes in 2010–2011 (a) and (b) 2006–2007. The red (green) bars indicate the DMI index during July–December in 2011 (2007). (c) Scatterplots of the DMI and ONI indexes (July–December) during 1982–2018 with the rare co-occurrences of pIOD and La Niña in 2011 (red) and 2007 (green). The shaded gray color indicates that the absolute values of the DMI and ONI indexes are smaller than 0.5°C .

with the anomalies in normal pIOD years (Figures 6a; Du et al., 2020; Gnanaseelan et al., 2012; Grunseich et al., 2011; Subrahmanyam et al., 2011; Thompson et al., 2006).

In the winter of 2011, the westerly wind anomaly related to La Niña favored downwelling Kelvin waves propagating from the eastern EIO into the BoB and then formed a cyclonic circulation anomaly in the bay (Figures 9b and 9d). Therefore, a positive SSSA extended eastward to the eastern EIO and then extended into the BoB (Figure 9d). Notably, a large negative SSSA (<-1.0 psu) was noted in the northern BoB. These SSSA features reflect that the cyclonic circulation anomaly transported salty water into the eastern EIO and BoB and transported freshwater from the eastern BoB to the northern bay.

The circulation and SSS anomalies during the fall to winter in 2011 can be explained as follows. In the fall of 2011, the anticyclonic circulation anomaly led to a weakened EICC that inhibited the southward freshwater transport along the eastern Indian coast. In the following winter, the cyclonic circulation anomaly prevented the transport of freshwater from the eastern BoB into the EIO. Thus, the freshwater in the BoB received during the summer monsoon of 2011 was inhibited from being transported out of the western bay during fall, and from being transported out of the eastern bay during winter. As a result, substantial freshwater was trapped and confined to the northern BoB by the end of winter (Figure 9d).

3.2.3. P-E and River Discharge Anomalies in 2011

During the summer monsoon (June–September, JJAS), local freshwater fluxes from P-E and river discharge contribute to low salinity values in the northern BoB (Akhil et al., 2014; Han et al., 2001; Pant et al., 2015; Papa et al., 2012). Therefore, it is necessary to investigate the contributions of P-E and river discharge anomalies to the extremely low salinity anomaly in the BoB during 2012 spring. To achieve this goal, the P-E and river discharge anomalies in the northern BoB during the summer of 2011 are quantified first. Then, the freshwater fluxes and SSS anomalies in 2011 are compared with those in a normal pIOD year, 2006.

Figures 10a and 10c show the P-E and SSS anomalies in the BoB during the summer of 2011. A positive P-E anomaly was noted in the northern BoB (Figure 10a), which can be attributed to the excess rainfall associated with the pIOD 2011. The rainfall anomaly was characterized by a slanting structure from the Myanmar to the northeastern Indian continent (Figure S1a). This particular anomaly pattern reflects the influence of the pIOD 2011 on the rainfall, as shown in comparison with that in 2006, a normal pIOD year (Figure S1b), and in several previous studies (Ashok et al., 2001; Behera et al., 1999; Pant et al., 2015). Consequently, a

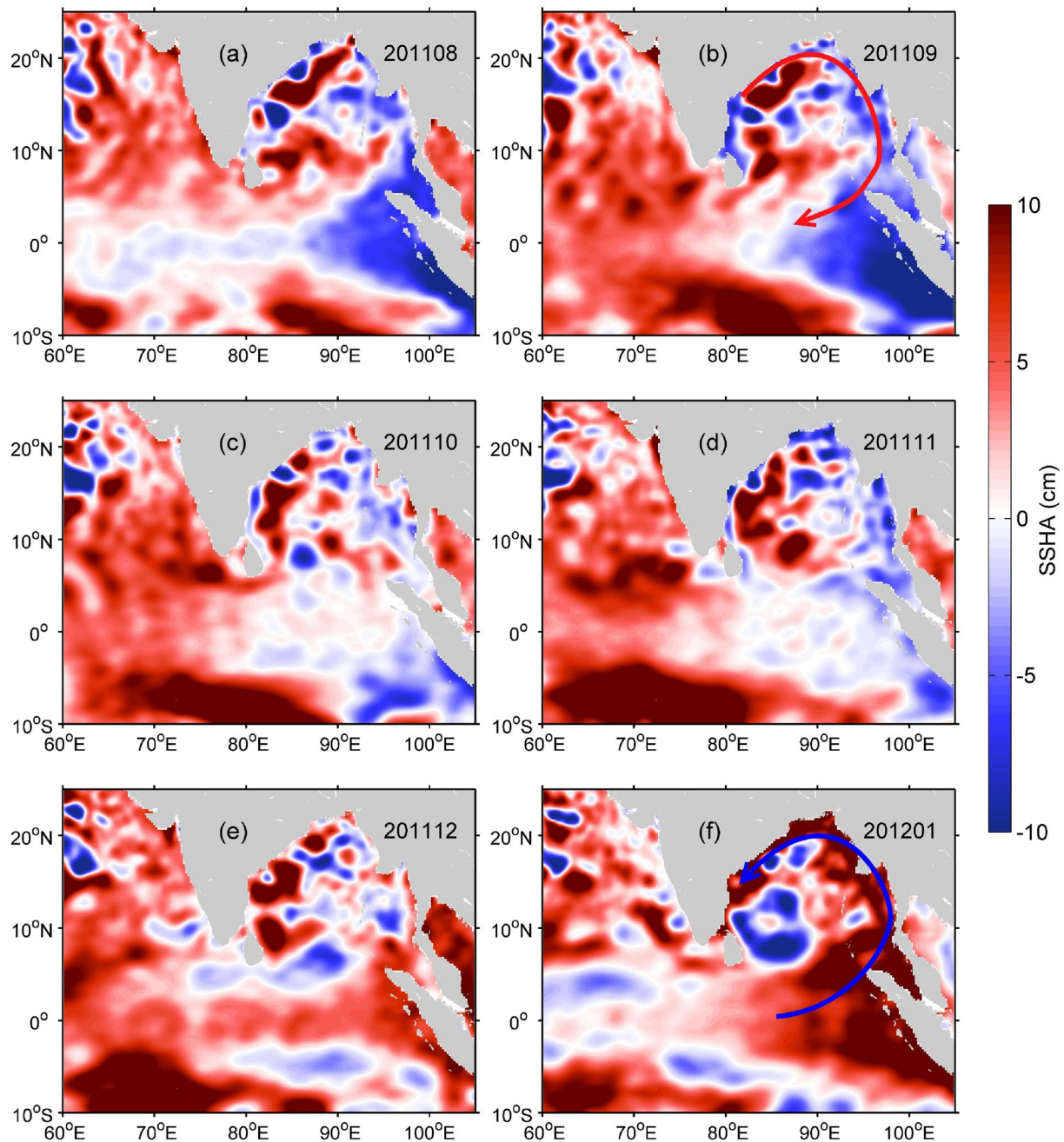


Figure 8. Monthly CMEMS SSHA in the BoB and eastern EIO from August 2011 to January 2012. The red (blue) arrows schematically indicate the anticyclonic (cyclonic) circulation anomaly.

negative SSSA was noted in the northern BoB (Figure 10c). This reflects that the pIOD 2011 caused a positive P-E anomaly that contributed to a negative SSSA in the northern BoB during summer.

Figures 10b and 10d show the P-E and SSS anomalies during the summer of 2006 for comparison with those in 2011. In the normal pIOD year 2006, the P-E anomaly shows a similar spatial pattern with that in 2011 although their magnitudes are different. Quantitatively, the area-averaged P-E anomaly over the northern BoB (north of 15°N) was 0.95 mm/day in 2011 and 1.63 mm/day in 2006. This can explain why the negative SSSA in the northern BoB during the summer in 2006 was lower than that in 2011 (Figure 10d). It is confirmed from the anomalies in 2006 and 2011 that the extremely low salinity anomaly in the BoB during 2012 spring cannot be mainly attributed to the P-E anomaly during the summer of 2011. This is explained

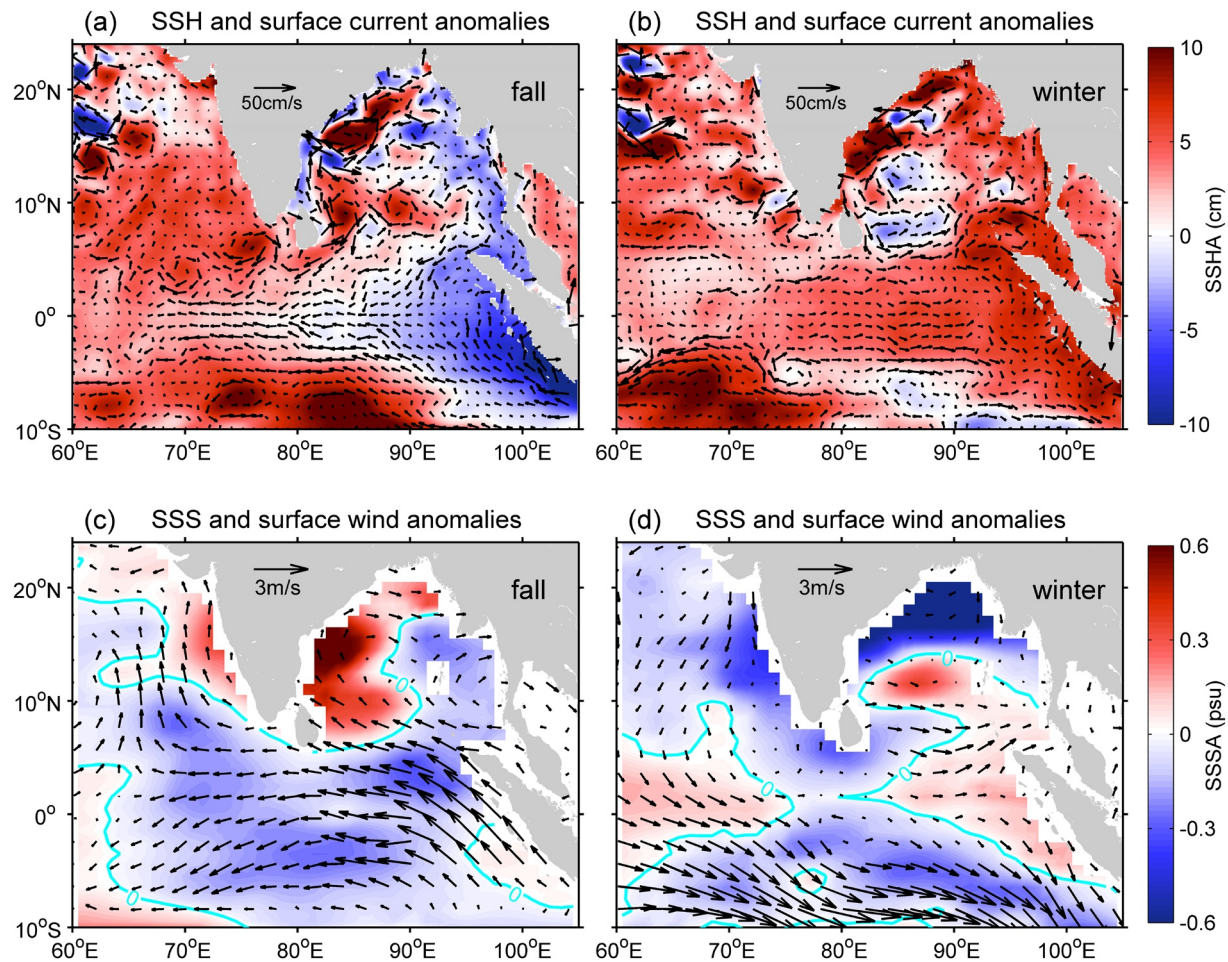


Figure 9. Anomalies of CMEMS SSH (color) and surface current (vector) and CCMP surface wind (vector) and Argo SSS (color) during the fall to winter in 2011.

as follows: if the spring SSSA in the northern BoB is mainly dominated by the P-E anomaly during the summer of a previous year, a lower negative SSSA should have occurred during 2007 spring. However, the spring SSSA in the northern BoB was much lower in 2012 than in 2007 (Figure 5f). This strongly suggests that other processes were responsible for forming the extremely low salinity anomaly during 2012 spring.

In addition to P-E, the discharge from the GB and Irrawaddy rivers also influences the SSS in the BoB. We investigate the river discharge anomaly in 2011 (Figure 11) to quantify its contribution to the extremely low salinity anomaly during 2012 spring. The sum of discharge from the GB and Irrawaddy rivers shows clear interannual variability. In 2011, however, we cannot recognize an evident enhancement in river discharge compared with the other years (Figure 11a). Quantitatively, the river discharge averaged during JJAS in 2011 was only 6.5% more than the climatological state (Figure 11b). Pant et al. (2015) showed that the sum of discharge from the major rivers in the BoB shows no significant difference between the pIOD years and the climatology. Thus, we argue that the river discharge during the summer of 2011 played a small role in forming the extremely low salinity anomaly in the BoB during 2012 spring.

3.3. Seasonal Freshwater Transport During 2012 Spring

As shown in Figure 9d, substantial freshwater was confined to the northern BoB by the end of the winter in 2011. How was this substantial freshwater in the northern BoB transported into the central and southern bay that formed the extremely low salinity anomaly in the spring of 2012? Figure 12a presents the standard deviation (STD) of the SSS, which reflects the freshwater transport in the BoB. The STD of the weekly

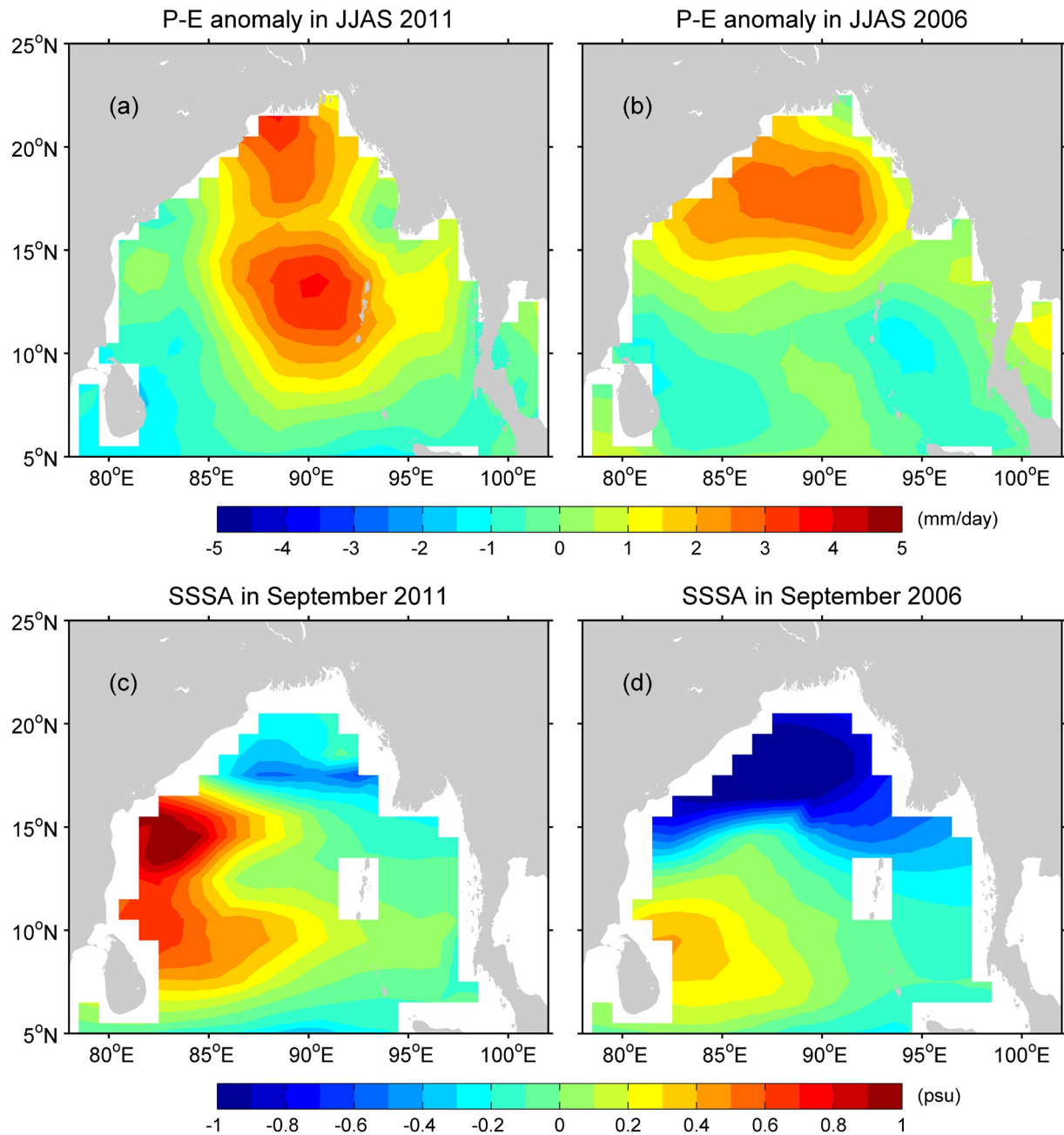


Figure 10. P-E anomaly in the BoB averaged from July to September in 2011 (a) and (b) 2006 based on the GPCP and OAflux data from 1979 to 2018. Argo September SSSA in the BoB in 2011 (c) and (d) 2006.

Aquarius OISS data clearly shows large values in the northern BoB and southeastern AS. Interestingly, a strip of high SSS STD values connecting the northeastern BoB coastal area to the south of Sri Lanka is noticeable (Section S1 in Figure 12a), reflecting the exchange of freshwater and salty water between the BoB and AS as indicated by Han and McCreary (2001) and Jensen (2001). The monthly Aquarius OISS and CMEMS surface current averaged during February to April show that an organized anticyclonic circulation transports freshwater from the northeastern BoB coastal area into the central and southern bay and then into the AS (Figure 12b). Consequently, the large SSS STD along Section S1 reflects the second freshwater pathway in the BoB during spring as indicated by Han and McCreary (2001) and Jensen (2001, 2007).

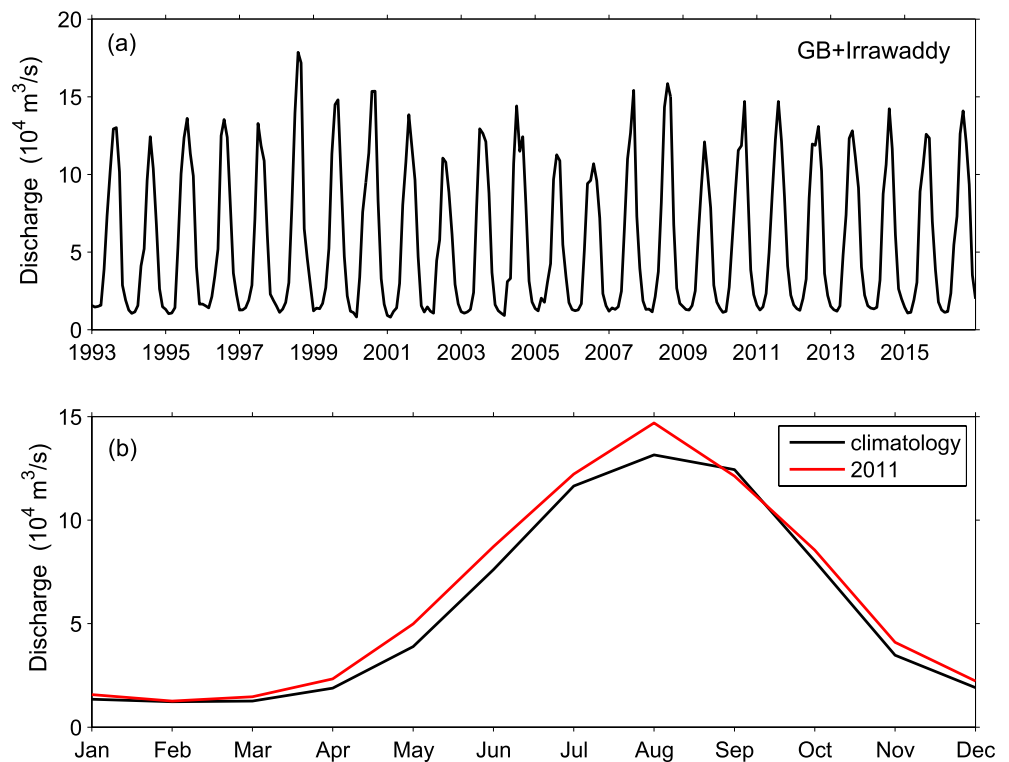


Figure 11. (a) Monthly evolution of river discharge from the BG and Irrawaddy rivers from 1993 to 2016. (b) Time series of monthly river discharge for the climatology (black) and 2011 (red).

This indicates that the extremely low salinity anomaly is due to the clockwise freshwater transport in the northern BoB by the anticyclonic circulation during spring. This freshwater transport is clearly evidenced from the SSS along Section S1 (Figures 12c and 12d). The freshwater transport started in January 2012 and ended in April. In particular, the SSS reached the minimum in March 2012 near 15°N, thus forming the extremely low salinity anomaly observed by the RAMA buoy at station B15. This freshwater transport can be further illustrated from the consecutive snapshots of weekly Aquarius OISSS, which clearly show clockwise freshwater transport in the northern and western BoB in the spring of 2012 (Figure 13).

3.4. Mixed Layer Salt Budget in the BoB

To illustrate the dominant processes controlling the mixed layer salinity variability in the BoB, the salt budget terms in Equation 1 are estimated using the climatology ORAS5 products (Figure 14). To better understand the spatial patterns of these terms, the annual cycle of ORAS5 current and salinity vertically averaged in the mixed layer are shown (Figure S2). The current and salinity show strong seasonal variations in the BoB, especially in the western side. One of the most prominent features of the current is the reversal of the EICC along the western boundary of the BoB. During October to December, the EICC flows southward along the eastern Indian coast (Figures S2j–S2l). Then, it reverses to northward during February to April, forming an anticyclonic gyre in the northern and western BoB (Figures S2b–S2d). For the salinity, the most striking feature is that low salinity freshwater occurs in the northern BoB during summer (Figures S2h). Then, the freshwater spreads southward along the eastern Indian coast during fall to winter (Figures S2i–S2l).

From an overall view, the salt budget clearly shows that the tendency term (Figures 14a1–14a4) and horizontal advection term (Figures 14c1–14c4) have the largest magnitudes throughout the whole year. Moreover, these two terms have very similar spatial patterns, indicating an overwhelming balance between each other. In contrast, the local freshwater flux term has a much smaller magnitude. A relatively larger magnitude of the local freshwater flux term can only be seen in the northern BoB during summer (Figure 14b3). This

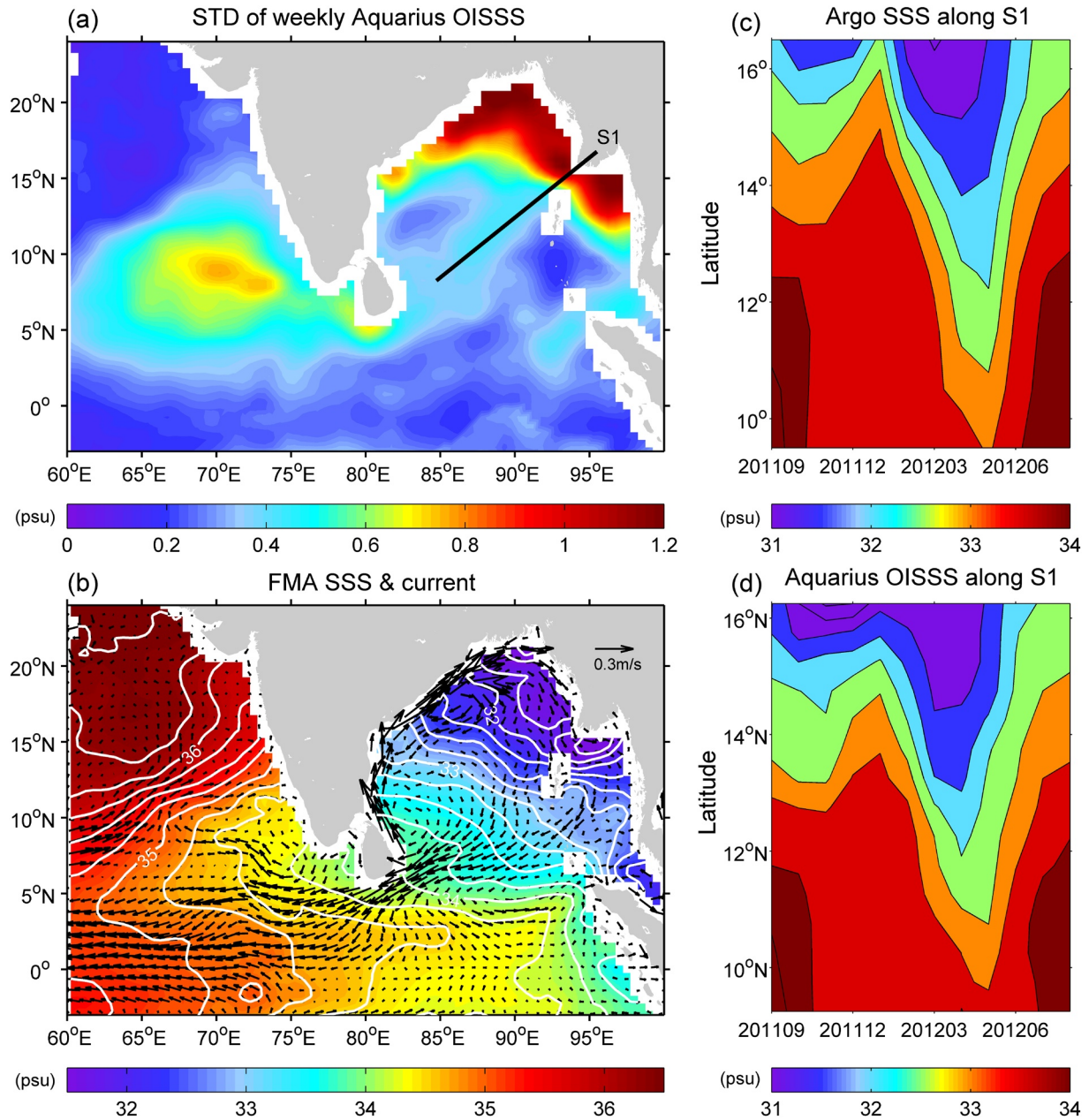


Figure 12. (a) STD of weekly Aquarius OISSS from August 27, 2011 to May 28, 2015. The black line indicates Section S1 from the northeastern BoB coastal area to the south of Sri Lanka. (b) Monthly Aquarius OISSS (2012–2015) overlapped with CMEMS surface current (1993–2018) averaged during February to April (FMA). Time-latitude plots of monthly Argo SSS (c) and Aquarius OISSS (d) along Section S1 from September 2011 to August 2012.

indicates that the local freshwater flux term contributes to the mixed layer salinity variability only during summer (Figures 14b1, 14b2 and 14b4). In summary, the salt budget analysis confirms that the horizontal advection plays a dominant role in controlling the mixed layer salinity variability in the BoB, which is consistent with the findings in previous studies (Akhil et al., 2014; Pant et al., 2015; R. Rao & Sivakumar, 2003; Roman-Stork et al., 2020).

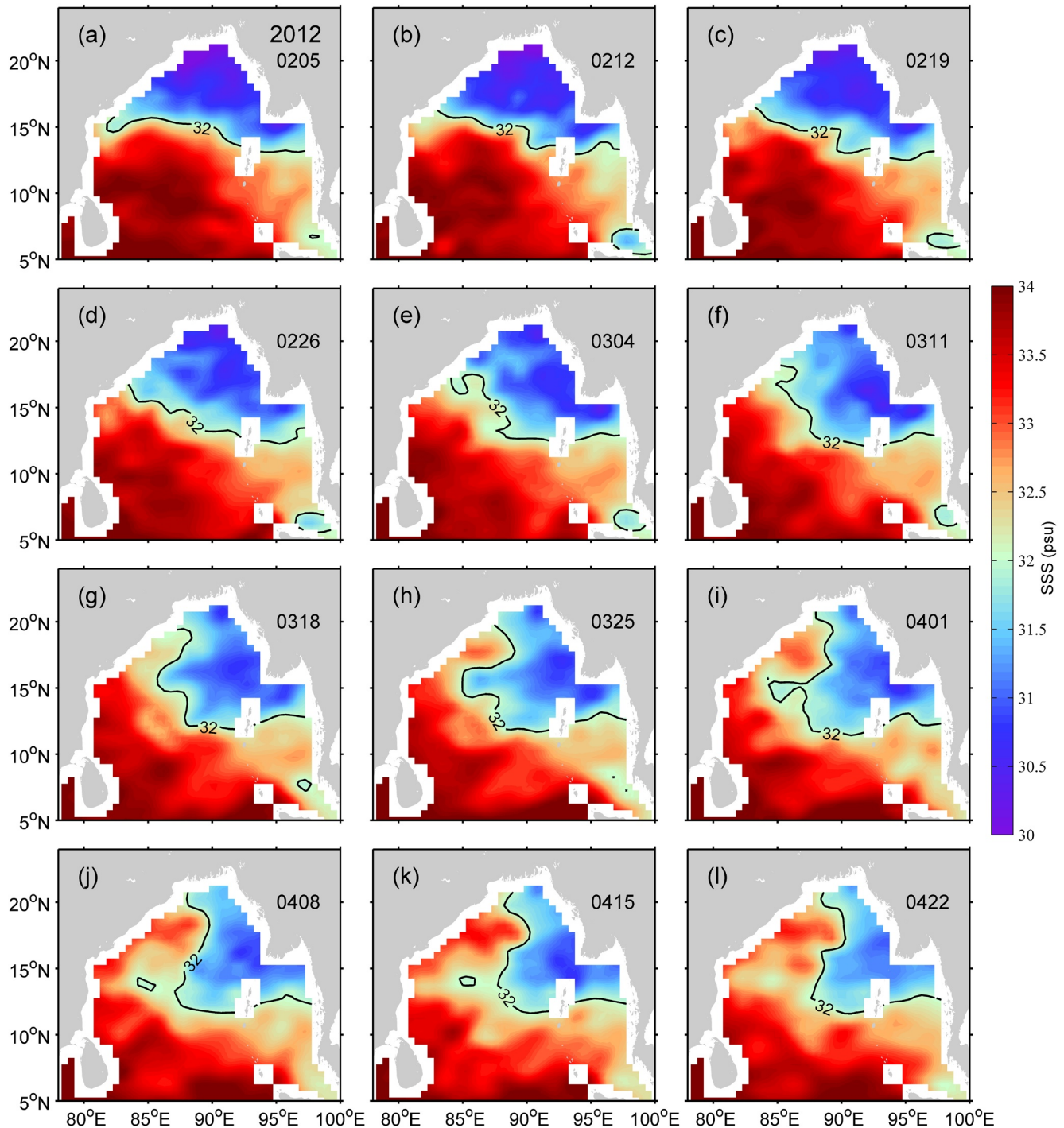


Figure 13. Consecutive snapshots of weekly Aquarius OISS from February 5 to April 22, 2012. The black line denotes the SSS contour of 32 psu.

4. Discussion

4.1. Freshwater Transport in the BoB During Spring

The BoB receives a large amount of freshwater during the summer monsoon (Figure 1c). This freshwater is transported by the basin-scale circulation, leading to strong seasonal SSS variability in the BoB (Akhil et al., 2014; Fournier et al., 2017; Z. Li et al., 2021; Murty et al., 1992; R. Rao & Sivakumar, 2003; Sengupta et al., 2016; Shetye et al., 1996; Suneel et al., 2020). The RAMA buoys at stations B15 (15°N, 90°E) and B12

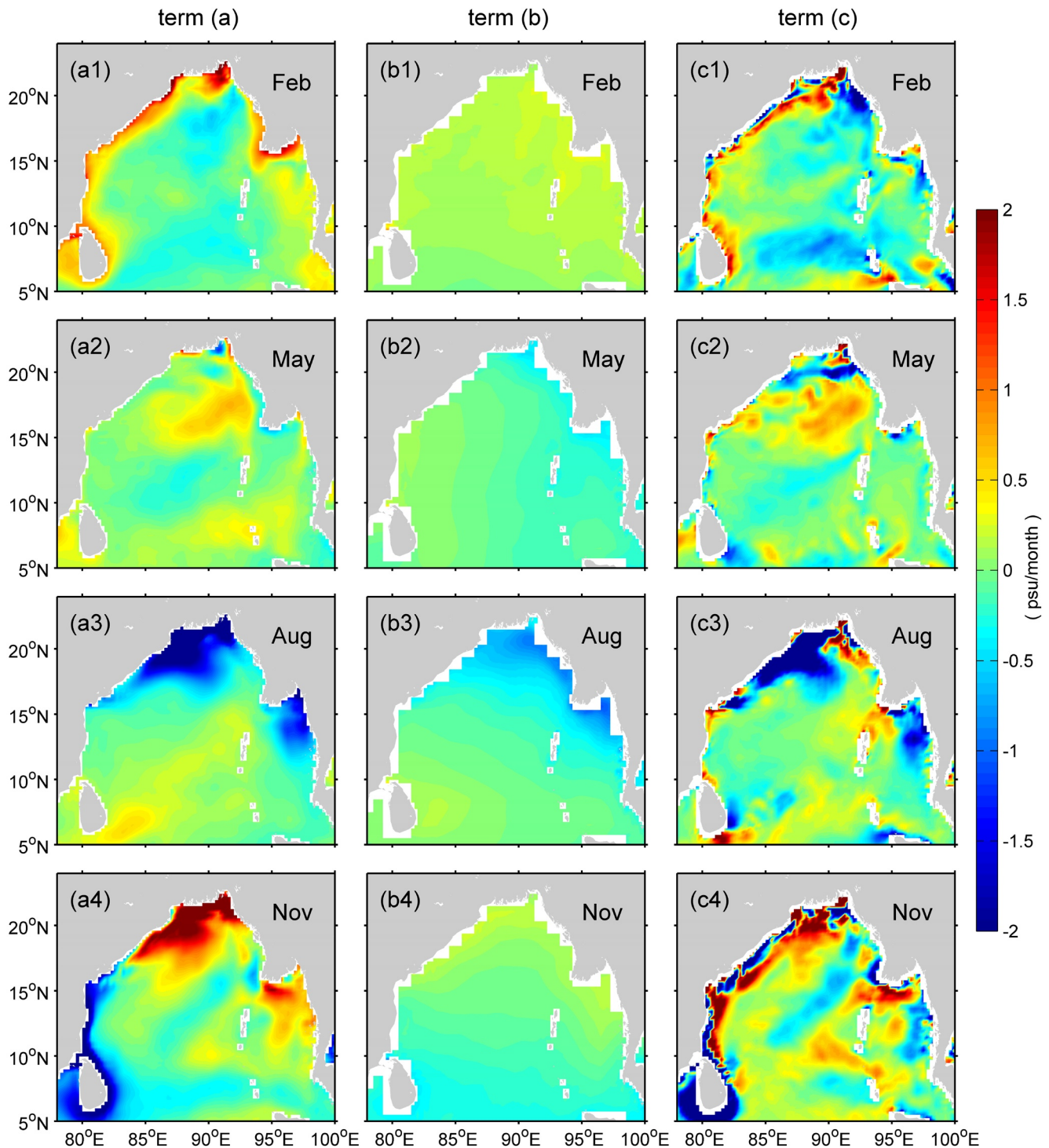


Figure 14. Spatial patterns of the tendency term (a1–a4), local freshwater flux term (b1–b4) and horizontal advection term (c1–c4).

(12°N, 90°E) provide high quality, vertically resolved data over long time periods that are important to understand the freshwater movements in the BoB. Uncommonly, an extremely low salinity anomaly was observed from the two RAMA buoys in the spring of 2012 (Figure 3). Our observational results show that the extremely low salinity anomaly in the spring of 2012 was caused by the clockwise transport of substantial freshwater in the BoB that can further trace back to strong seasonal anticyclonic circulation (Figures 12 and 13), which verifies the model results proposed by Han and McCreary (2001) and Jensen (2001, 2007).

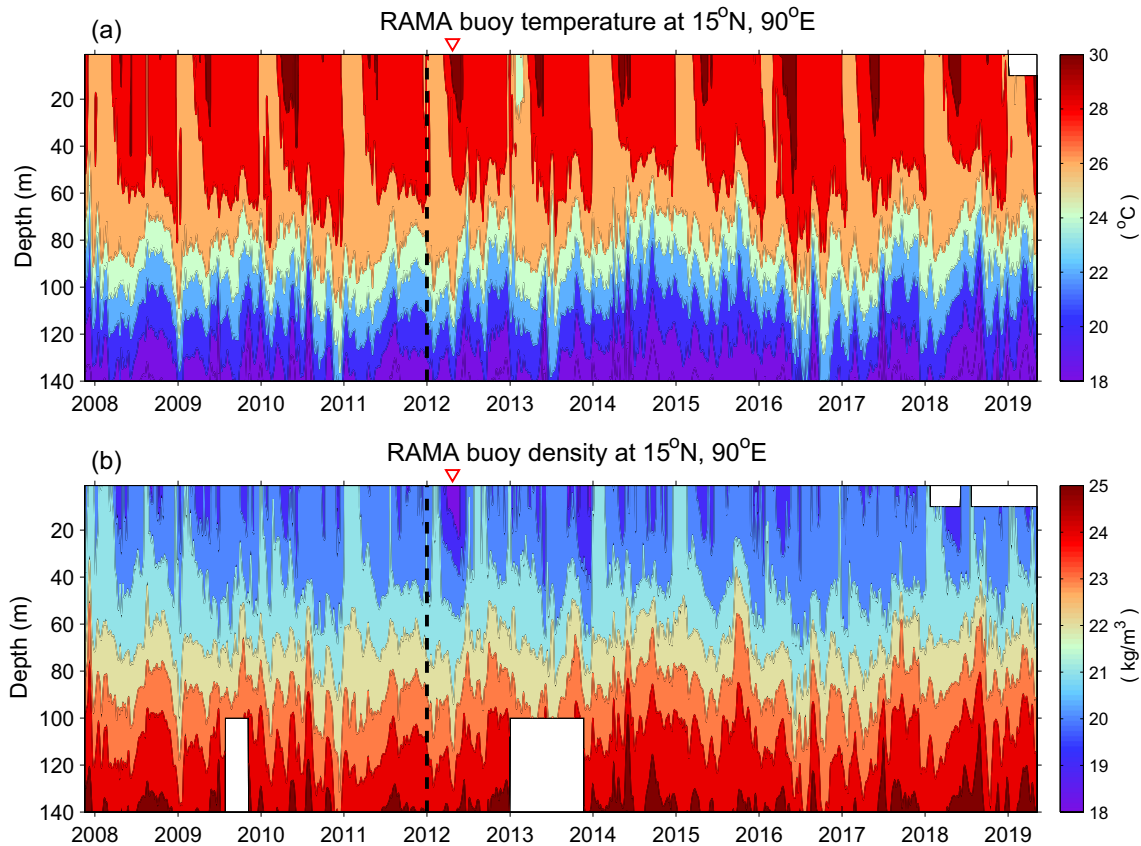


Figure 15. 10-day smoothed daily temperature (a) and (b) potential density measured by the RAMA buoy at station B15. The black dashed line indicates the year 2012, and the red triangle highlights the extremely low salinity anomaly in the spring of 2012.

Interestingly, the Aquarius OISS identifies a strip of high STD values of SSS connecting the northeastern BoB to the south of Sri Lanka (Figure 12a), which may be an indicator of the freshwater pathway in the BoB during spring.

Combined with the spatial pattern and vertical profile of the extremely low salinity anomaly, a thick layer of freshwater was transported into the central and southern bay (Figures 3 and 5). This substantial freshwater flux is vital to the freshwater exchange between the BoB and AS (Behara et al., 2019; Lasitha Perera et al., 2019; Trott et al., 2019) and can further influence the monsoon onset and strength (Nyadjro et al., 2011; Roman-Stork et al., 2020). Moreover, the BoB experiences the coldest sea temperature in winter and the warmest sea temperature in spring (Figure 15a), indicating a huge heat exchange in the mixed layer during this period. This extremely low salinity anomaly caused very strong near-surface stratification (Figure 15b), which significantly influenced the thermodynamics in the mixed layer. Further research on the influence of this substantial freshwater flux on the mixed layer thermodynamics in the BoB is needed.

4.2. Modulation by a Rare Co-Occurrence of pIOD and La Niña in 2011

During the summer of 2011, the P-E in the northern BoB and sum of discharge from the GB and Irrawaddy rivers show positive anomalies with respect to their climatological states (Figures 10 and 11). These excessive local freshwater fluxes contributed to a low salinity freshwater (negative SSSA) in the northern BoB during the summer of 2011 (Figure 10c). While, the comparison of the P-E and SSS anomalies between 2011 and 2006 strongly suggests that the extremely low salinity anomaly in the BoB during 2012 spring cannot be mainly attributed to the anomalous local freshwater fluxes during the summer of 2011. In contrast, the anomalous freshwater transport in the BoB was responsible for forming the extremely low salinity anomaly, as indicated by the mixed layer salt budget (Figure 14).

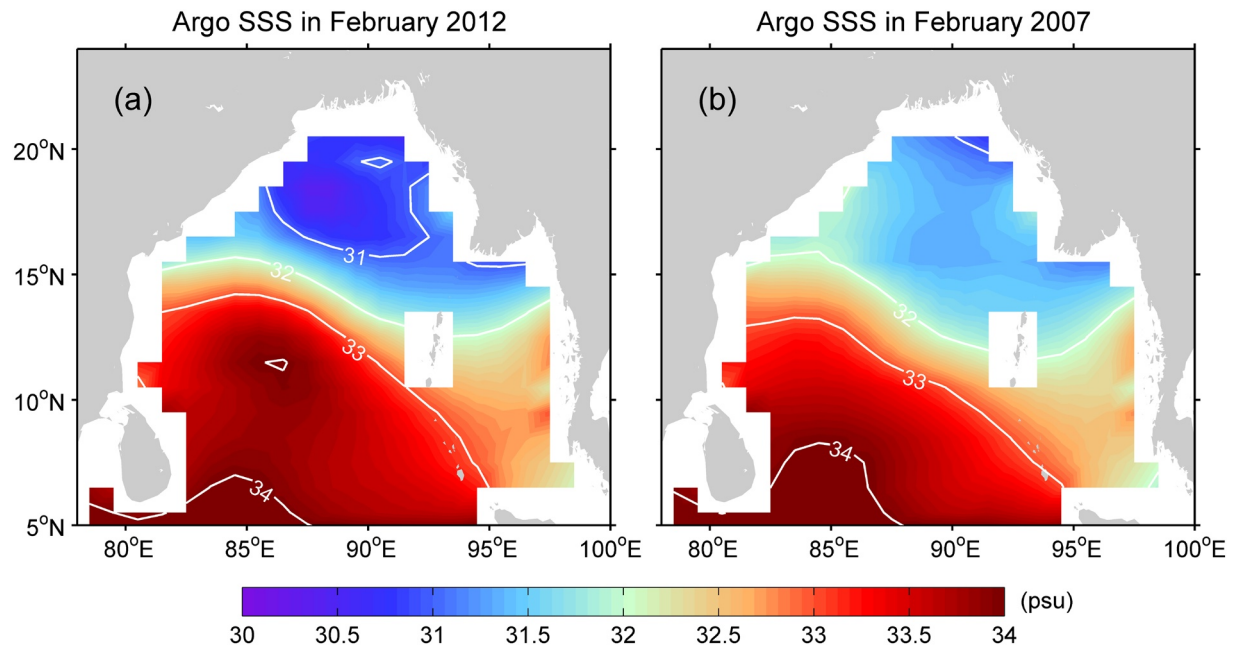


Figure 16. Argo February SSS distribution in the BoB in 2012 (a) and (b) 2007.

A key formation mechanism of the extremely low salinity anomaly is the circulation modulated by a rare co-occurrence of pIOD and La Niña in 2011. A distinct difference in the circulation anomaly between the combination event 2011 and the normal pIOD years is that the anticyclonic pattern reversed to a cyclonic pattern flowing from the eastern EIO into the BoB during the winter of 2011 (Figure 9b). The cyclonic circulation anomaly was generated by the equatorial westerly wind anomaly related to the La Niña event (Figures 9b and 9d). These reversing circulation anomalies significantly influenced the freshwater transport in the BoB in 2011: the freshwater in the northern BoB was inhibited from being transported out of the western bay during fall, and from being transported out of the eastern bay during winter. As a result, substantial freshwater was trapped and confined to the northern bay by the end of winter (February of the next year). For example, the February SSS distribution in the northern BoB was much lower in 2012 than 2007 (Figure 16). These circulation and SSS anomaly features in the BoB during the co-occurrence of pIOD and La Niña in 2011 are different from those in the normal pIOD years (Akhil et al., 2016; Fournier et al., 2017; Grunseich et al., 2011; Pant et al., 2015). Our findings can explain why the negative SSSA in the northern BoB was even more significant during a moderate pIOD 2011 than during a strong pIOD 2006 (Figures 3 and 4 in Pant et al., 2015). We argue that the role of La Niña in the SSS interannual variability in the BoB in 2011 cannot be neglected. The pIOD 2011 followed a nIOD 2010 (Figure 7a), which is usual in IOD variability (Behera et al., 2006, 2008; Saji et al., 1999). Thus, this rare co-occurrence of pIOD and La Niña in 2011 can largely be attributed to the La Niña event 2010/2011, which was so strong and influential worldwide (Boening et al., 2012). In the future, the reasons for the formation of this rare co-occurrence of pIOD and La Niña in 2011 and its influences on the SST and thermocline depth anomalies in the EIO need further investigation.

It is interesting that another co-occurrence of pIOD and La Niña occurred in 2007 (Figures 7b and 7c). However, one cannot identify a significant low SSSA in the BoB during the spring of 2008 (Figure 5f). Our analysis has confirmed that the SSS variability in the BoB is dominated by the horizontal advection due to local circulation (Figure 14). This motivates us to check out the circulation anomaly differences in the BoB between 2007 and 2011. During the peak phase of the pIOD 2007, large area of negative SSHA was found in the BoB (Figures 17c–17g). Thus, the organized anticyclonic circulation anomaly pattern shown in both the normal pIOD years and the combination event 2011 cannot be recognized in 2007. Although, a cyclonic circulation anomaly pattern flowing from the eastern EIO into the BoB can be found in the following winter (reflecting the dominant role of the La Niña event 2007). These features mean that the reversing circulation anomalies during the fall to winter in 2011 were not presented in 2007. This is why no significant low SSSA

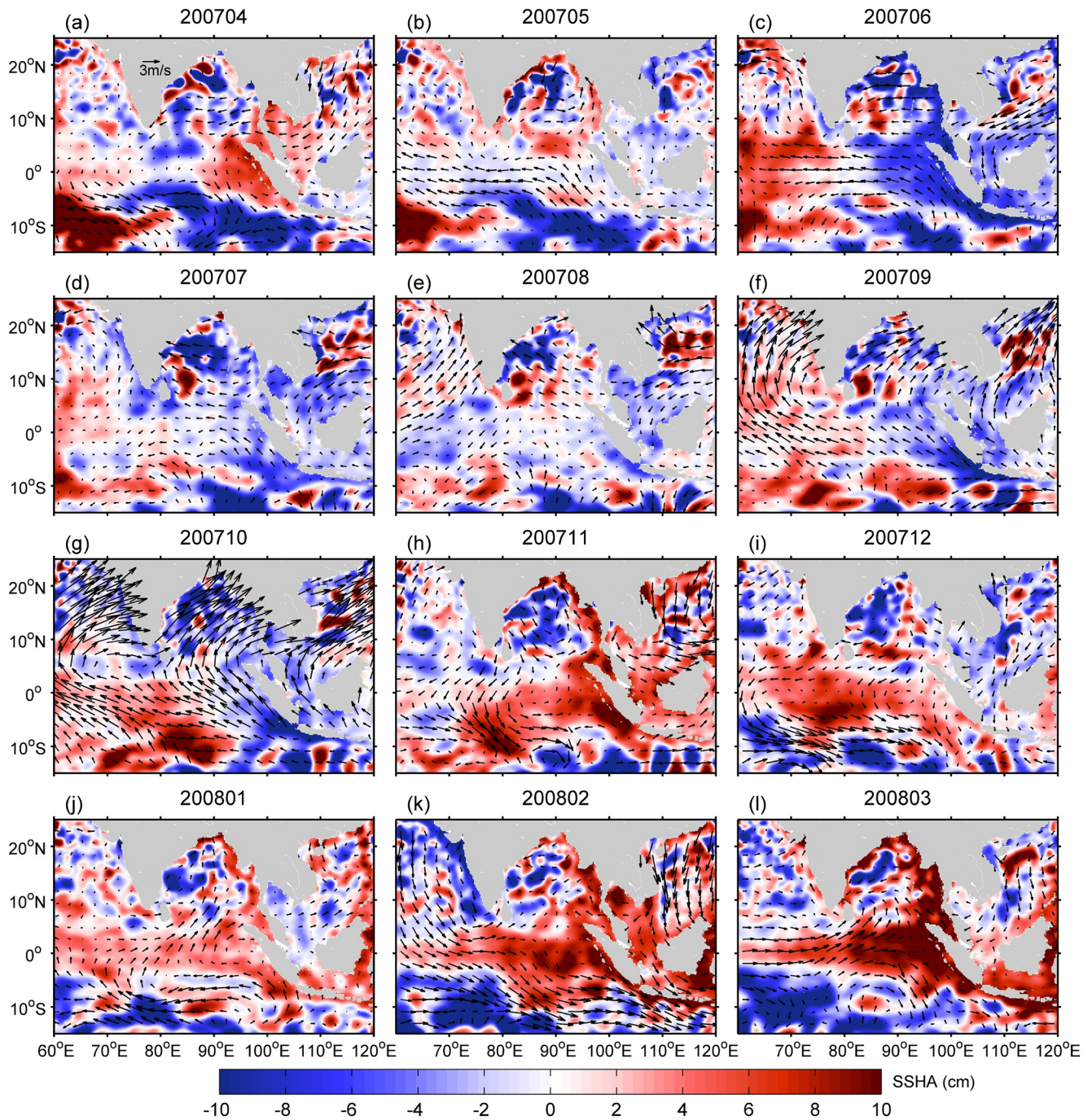


Figure 17. Anomalies of CMEMS SSH (color) and CCMP surface wind (arrows) from April 2007 to March 2008.

was found in the BoB during the spring of 2008. As shown in Figure 7, the pIOD 2007 event followed another pIOD event 2006, which is evidently different from the pIOD 2011 that followed a nIOD 2010. Behera et al. (2008) concluded that “the atmospheric conditions with subsidence over the Maritime Continent caused divergent easterly wind anomalies in the eastern EIO to trigger the consecutive pIOD event 2007 through oceanic dynamics”. As shown in Figures 17c–17g, these divergent wind anomalies were responsible for the large area of negative SSHA in the BoB, the eastern EIO and the Maritime Continent.

5. Summary

This study reveals an extremely low salinity anomaly in the BoB based on various in situ and satellite observations in the spring of 2012 and discusses its spatial characteristics and formation mechanisms. The extremely low salinity anomaly featured a long time, large-scale, and deep depth throughout the whole BoB and was ranked as the strongest springtime low salinity anomaly in the last two decades. The results show that the anomalous freshwater transport in the BoB during a rare co-occurrence of pIOD and La Niña in 2011 was the main cause of this extreme event. During the fall to winter in 2011, the anticyclonic circulation anomaly reversed to a cyclonic pattern that inhibited the southward freshwater transport along the two sides of the BoB. As a result, substantial freshwater was trapped and confined to the northern bay by the end of winter. This freshwater was transported by the subsequent strong seasonal anticyclonic circulation into the central and southern bay, forming the extremely low salinity anomaly in the spring of 2012. The key process was the modulation of the seasonal monsoon by interannual processes, specifically the rare combination of pIOD and La Niña in 2011. Our results highlight the important role of the oceanic circulation in the SSS variability in the BoB. This study provides some new perspectives on the SSS interannual variability in the BoB and the freshwater exchange between the BoB and the AS.

Data Availability Statement

The multi-satellite merged SSH L4 product are provided by the CMEMS at <http://marine.copernicus.eu/>. The DMI and Argo data are provided by the JAMSTEC at <http://www.jamstec.go.jp>, and the ONI data are provided by the NOAA-CPC at https://origin.cpc.ncep.noaa.gov/products/analysis_monitoring/ensostuff/ONI_v5.php. The Version 2 CCMP surface wind data are provided by the remote sensing system at <http://www.remss.com/measurements/ccmp/>.

Acknowledgments

We thank the anonymous reviewers for their valuable comments that greatly improved the manuscript. This study was supported by the National Natural Science Foundation of China (grant numbers 41920104006, 41776107), the Scientific Research Fund of SIO, MNR (JZ2001, QNYC2001), the Indo-Pacific Ocean Variability and Air-Sea Interaction (GASI-01-WPAC-STspr), the Project of State Key Laboratory of Satellite Ocean Environment Dynamics, SIO (SOEDZZ2106), the Scientific research foundation of Zhejiang University of Water Resources and Electric Power and the open fund of State Key Laboratory of Satellite Ocean Environment Dynamics, Second Institute of Oceanography, MNR (QNHX2114). The authors acknowledge the NOAA Pacific Marine Environmental Laboratory for providing the RAMA mooring data at <https://www.pmel.noaa.gov> and the APDRC-IPRC for providing the Aquarius OISSS data at <http://apdrc.soest.hawaii.edu>.

References

- Adler, R., Huffman, G., Chang, A., Ferraro, R., Xie, P., Janowiak, J., et al. (2003). The version-2 global precipitation climatology project (GPCP) monthly precipitation analysis (1979–present). *Journal of Hydrometeorology*, 4(6), 1147–1167. [https://doi.org/10.1175/1525-7541\(2003\)004<1147:Tvgpcp>2.0.Co;2](https://doi.org/10.1175/1525-7541(2003)004<1147:Tvgpcp>2.0.Co;2)
- Akhil, V., Durand, F., Lengaigne, M., Vialard, J., Keerthi, M., Gopalakrishna, V., et al. (2014). A modeling study of the processes of surface salinity seasonal cycle in the Bay of Bengal. *Journal of Geophysical Research: Oceans*, 119, 3926–3947. <https://doi.org/10.1002/2013JC009632>
- Akhil, V., Lengaigne, M., Vialard, J., Durand, F., Keerthi, M., Chaitanya, A., et al. (2016). A modeling study of processes controlling the Bay of Bengal sea surface salinity interannual variability. *Journal of Geophysical Research: Oceans*, 121, 8471–8495. <https://doi.org/10.1002/2016JC011662>
- Ashok, K., Guan, Z., & Yamagata, T. (2001). Impact of the Indian Ocean Dipole on the decadal relationship between the Indian monsoon rainfall and ENSO. *Geophysical Research Letter*, 28, 4499–4502. <https://doi.org/10.1029/2001gl013294>
- Atlas, R., Hoffman, R., Ardizzone, J., Leidner, S., Jusem, J., Smith, D., & Gombos, D. (2011). A cross-calibrated, multiplatform ocean surface wind velocity product for meteorological and oceanographic applications. *Bulletin of the American Meteorological Society*, 92, 157–174. <https://doi.org/10.1175/2010BAMS2946.1>
- Behara, A., Vinayachandran, P., & Shankar, D. (2019). Influence of rainfall over eastern Arabian Sea on its salinity. *Journal of Geophysical Research: Oceans*, 124, 5003–5020. <https://doi.org/10.1029/2019JC014999>
- Behera, S., Krishnan, R., & Yamagata, T. (1999). Unusual ocean-atmospheric conditions in the tropical Indian Ocean during 1994. *Geophysical Research Letter*, 26, 3001–3004. <https://doi.org/10.1029/1999gl010434>
- Behera, S., Luo, J., Masson, S., Rao, S., Sakuma, H., & Yamagata, T. (2006). A CGCM study on the interaction between IOD and ENSO. *Journal of Climate*, 19, 1608–1705. <https://doi.org/10.1175/jcli3797.1>
- Behera, S., Luo, J., & Yamagata, T. (2008). Unusual IOD event of 2007. *Geophysical Research Letter*, 35, L14S11. <https://doi.org/10.1029/2008GL034122>
- Boening, C., Willis, J., Landerer, F., Nerem, R., & Fasullo, J. (2012). The 2011 La Niña: So strong, the oceans fell. *Geophysical Research Letter*, 39, L19602. <https://doi.org/10.1029/2012GL053055>
- Cai, W., Pan, A., Roemmich, D., Cowan, T., & Guo, X. (2009). Argo profiles a rare occurrence of three consecutive positive Indian Ocean Dipole events, 2006–2008. *Geophysical Research Letter*, 36, L08701. <https://doi.org/10.1029/2008GL037038>
- Chaitanya, A. V. S., Lengaigne, M., Vialard, J., Gopalakrishna, V. V., Durand, F., KranthiKumar, C., et al. (2014). Salinity measurements collected by fishermen reveal a “river in the sea” flowing along the Eastern Coast of India. *Bulletin of the American Meteorological Society*, 95, 1897–1908. <https://doi.org/10.1175/BAMS-D-12-00243.1>
- Chen, G., Han, W., Li, Y., & Wang, D. (2016). Interannual variability of equatorial eastern Indian Ocean upwelling: Local versus remote forcing. *Journal of Physical Oceanography*, 46, 789–807. <https://doi.org/10.1175/JPO-D-15-0117.1>
- Chen, G., Han, W., Li, Y., Wang, D., & Shinoda, T. (2015). Intraseasonal variability of upwelling in the equatorial eastern Indian Ocean. *Journal of Geophysical Research: Oceans*, 120, 7598–7615. <https://doi.org/10.1002/2015JC011223>
- Du, Y., & Zhang, Y. (2015). Satellite and Argo observed surface salinity variations in the tropical Indian Ocean and their association with the Indian Ocean Dipole mode. *Journal of Climate*, 28(2), 695–713. <https://doi.org/10.1175/JCLI-D-14-00435.1>
- Du, Y., Zhang, Y., Zhang, L., Tozuka, T., Ng, B., & Cai, W. (2020). Thermocline warming induced extreme Indian Ocean dipole in 2019. *Geophysical Research Letters*, 47, e2020GL090079. <https://doi.org/10.1029/2020GL090079>

- Fore, A., Yueh, S., Tanh, W., & Hayashi, A. (2020). *JPL SMAP ocean surface salinity products [level 2B, level 3 running 8-day, level 3 monthly], version 5.0 validated release*. Pasadena: Jet Propulsion Laboratory.
- Fournier, S., Vialard, J., Lengaigne, M., Lee, T., Gierach, M., & Chaitanya, A. (2017). Modulation of the GangesBrahmaputra river plume by the Indian Ocean dipole and eddies inferred from satellite observations. *Journal of Geophysical Research: Oceans*, *122*, 9591–9604. <https://doi.org/10.1002/2017JC013333>
- Girishkumar, M. S., Joseph, J., Thangaprakash, V. P., Pottapinjara, V., & McPhaden, M. J. (2017). Mixed layer temperature budget for the northward propagating Summer Monsoon Intraseasonal Oscillation (MISO) in the Central Bay of Bengal. *Journal of Geophysical Research: Oceans*, *122*, 8841–8854. <https://doi.org/10.1002/2017JC013073>
- Girishkumar, M. S., Ravichandran, M., & McPhaden, M. J. (2013). Temperature inversions and their influence on the mixed layer heat budget during the winters of 2006–2007 and 2007–2008 in the Bay of Bengal. *Journal of Geophysical Research: Oceans*, *118*, 2426–2437. <https://doi.org/10.1002/jgrc.20192>
- Gnanaseelan, C., Deshpande, A., & McPhaden, M. (2012). Impact of Indian Ocean Dipole and El Niño/Southern Oscillation wind-forcing on the Wyrkti jets. *Journal of Geophysical Research*, *117*, C08005. <https://doi.org/10.1029/2012JC007918>
- Grunseich, G., Subrahmanyam, B., Murty, V., & Giese, B. (2011). Sea surface salinity variability during the Indian Ocean Dipole and ENSO events in the tropical Indian Ocean. *Journal of Geophysical Research*, *116*, C11013. <https://doi.org/10.1029/2011JC007456>
- Han, W., & McCreary, J. (2001). Modeling salinity distributions in the Indian Ocean. *Journal of Geophysical Research*, *106*(C1), 859–877. <https://doi.org/10.1029/2000jc000316>
- Han, W., McCreary, J., & Kohler, K. (2001). Influence of precipitation minus evaporation and Bay of Bengal rivers on dynamics, thermodynamics, and mixed layer physics in the upper Indian Ocean. *Journal of Geophysical Research*, *106*, 6895–6916. <https://doi.org/10.1029/2000jc000403>
- Hong, C., Lu, M., & Kanamitsu, M. (2008). Temporal and spatial characteristics of positive and negative Indian Ocean dipole with and without ENSO. *Journal of Geophysical Research*, *113*, D08107. <https://doi.org/10.1029/2007JD009151>
- Hosoda, S., Ohira, T., & Nakamura, T. (2008). A monthly mean dataset of global oceanic temperature and salinity derived from Argo float observations. *JAMSTEC Report of Research and Development*, *8*, 47–59. <https://doi.org/10.5918/jamstecr.8.47>
- Huang, H., Wang, D., Yang, L., & Huang, K. (2021). Enhanced intraseasonal variability of the upper layers in the southern Bay of Bengal during the summer 2016. *Journal of Geophysical Research: Oceans*, *126*, e2021JC017459. <https://doi.org/10.1029/2021JC017459>
- Huffman, G., Adler, R., Bolvin, D., & Gu, G. (2009). Improving the global precipitation record: GPCP version 2.1. *Geophysical Research Letters*, *36*, L17808. <https://doi.org/10.1029/2009gl040000>
- Jensen, T. (2001). Arabian Sea and Bay of Bengal exchange of salt and tracers in an ocean model. *Geophysical Research Letter*, *28*, 3967–3970. <https://doi.org/10.1029/2001gl013422>
- Jensen, T. (2007). Wind-driven response of the Northern Indian Ocean to climate extremes. *Journal of Climate*, *20*(13), 2978–2993. <https://doi.org/10.1175/jcli4150.1>
- Lasitha Perera, G., Chen, G., McPhaden, M., Priyadarshana, T., Huang, K., & Wang, D. (2019). Meridional and zonal eddy-induced heat and salt transport in the Bay of Bengal and their seasonal modulation. *Journal of Geophysical Research: Oceans*, *124*, 8079–8101. <https://doi.org/10.1029/2019JC015124>
- Li, J., Liang, C., Tang, Y., Dong, C., Chen, D., Liu, X., & Jin, W. (2016). A new dipole index of the salinity anomalies of the tropical Indian Ocean. *Scientific Reports*, *6*, 24260. <https://doi.org/10.1038/srep24260>
- Li, Y., Han, W., Ravichandran, M., Wang, W., Shinoda, T., & Lee, T. (2017). Bay of Bengal salinity stratification and Indian summer monsoon intraseasonal oscillation: 1. Intraseasonal variability and causes. *Journal of Geophysical Research: Oceans*, *122*, 4291–4311. <https://doi.org/10.1002/2017JC012691>
- Li, Y., Han, W., Wang, W., Ravichandran, M., Lee, T., & Shinoda, T. (2017). Bay of Bengal salinity stratification and Indian summer monsoon intraseasonal oscillation: 2. Impact on SST and convection. *Journal of Geophysical Research: Oceans*, *122*, 4312–4328. <https://doi.org/10.1002/2017JC012692>
- Li, Z., Huang, S., Zhu, X., Sun, Z., Long, Y., & Xie, H. (2021). Short-term offshore extension of Brahmaputra–Ganges and Irrawaddy freshwater plumes to the central northern Bay of Bengal based on in situ and satellite observations. *Acta Oceanologica Sinica*, *40*(5), 80–93. <https://doi.org/10.1007/s13131-021-1729-y>
- Lian, T., Chen, D., Tang, Y., & Jin, B. (2014). A theoretical investigation of the tropical Indo-Pacific tripole mode. *Science China Earth Sciences*, *57*(1), 174–188. <https://doi.org/10.1007/s11430-013-4762-7>
- McPhaden, M., Meyers, G., Ando, K., Masumoto, Y., Murty, V. S. N., Ravichandran, M., et al. (2009). RAMA: The research moored array for African-Asian-Australian monsoon analysis and prediction. *Bulletin of the American Meteorological Society*, *90*, 459–480. <https://doi.org/10.1175/2008bams2608.1>
- Melnichenko, O., Hacker, P., Maximenko, N., Lagerloef, G., & Potemra, J. (2014). Spatial Optimal Interpolation of Aquarius sea surface salinity: Algorithms and implementation in the North Atlantic. *Journal of Atmosphere Oceanic Technology*, *31*, 1583–1600. <https://doi.org/10.1175/jtech-d-13-00241.1>
- Melnichenko, O., Hacker, P., Maximenko, N., Lagerloef, G., & Potemra, J. (2015). Optimum interpolation analysis of Aquarius sea surface salinity. *Journal of Geophysical Research: Oceans*, *121*. <https://doi.org/10.1002/2015JC011343>
- Murty, V. S. N., Sarma, Y. V. B., Rao, D. P., & Murty, C. S. (1992). Water characteristics, mixing and circulation in the Bay of Bengal during southwest monsoon. *Journal of Marine Research*, *50*(2), 207–228. <https://doi.org/10.1357/002224092784797700>
- Nyadjro, E., Subrahmanyam, B., & Shriver, J. (2011). Seasonal variability of salt transport during the Indian Ocean monsoons. *Journal of Geophysical Research*, *116*, C08036. <https://doi.org/10.1029/2011jc006993>
- Pant, V., Girishkumar, M., Udaya Bhaskar, T., Ravichandran, M., Papa, F., & Thangaprakash, V. (2015). Observed interannual variability of near-surface salinity in the Bay of Bengal. *Journal of Geophysical Research: Oceans*, *120*, 3315–3329. <https://doi.org/10.1002/2014JC010340>
- Papa, F., Bala, S., Pandey, R., Durand, F., Gopalakrishna, V., Rahman, A., & Rossow, W. B. (2012). Ganga–Brahmaputra river discharge from Jason-2 radar altimetry: An update to the long-term satellite-derived estimates of continental freshwater forcing flux into the Bay of Bengal. *Journal of Geophysical Research*, *117*, C11021. <https://doi.org/10.1029/2012JC008158>
- Papa, F., Durand, F., Rossow, W., Rahman, A., & Bala, S. (2010). Satellite altimeter derived monthly discharge of the Ganga–Brahmaputra River and its seasonal to interannual variations from 1993 to 2008. *Journal of Geophysical Research*, *115*, C12013. <https://doi.org/10.1029/2009JC006075>
- Parampil, S., Gera, A., Ravichandran, M., & Sengupta, D. (2010). Intraseasonal response of mixed layer temperature and salinity in the Bay of Bengal to heat and freshwater flux. *Journal of Geophysical Research*, *115*, C05002. <https://doi.org/10.1029/2009JC005790>
- Rao, R., & Sivakumar, R. (2003). Seasonal variability of sea surface salinity and salt budget of the mixed layer of the north Indian Ocean. *Journal of Geophysical Research*, *108*(C1), 3009. <https://doi.org/10.1029/2001JC000907>

- Rao, S., Saha, S., Pokhrel, S., Sundar, D., Dhakate, A., Mahapatra, S., et al. (2011). Modulation of SST, SSS over northern Bay of Bengal on ISO time scale. *Journal of Geophysical Research*, *116*, C09026. <https://doi.org/10.1029/2010JC006804>
- Roman-Stork, H., Subrahmanyam, B., & Murty, V. (2020). The role of salinity in the southeastern Arabian Sea in determining monsoon onset and strength. *Journal of Geophysical Research: Oceans*, *125*, e2019JC015592. <https://doi.org/10.1029/2019JC015592>
- Saji, N., Goswami, B., Vinayachandran, P., & Yamagata, T. (1999). A Dipole Mode in the Tropical Indian Ocean. *Nature*, *401*(6751), 360–363. <https://doi.org/10.1038/43855>
- Saji, N., & Yamagata, T. (2003). Possible impacts of Indian Ocean Dipole mode events on global climate. *Climate Research*, *25*(2), 151–169. <https://doi.org/10.3354/cr025151>
- Sengupta, D., Bharath, R., Ravichandran, M., Sree Lekha, J., & Papa, F. (2016). Near-surface salinity and stratification in the north Bay of Bengal from moored observations. *Geophysical Research Letters*, *43*, 4448–4456. <https://doi.org/10.1002/2016GL068339>
- Sengupta, D., Bharath, R., & Shenoi, S. (2006). Surface freshwater from Bay of Bengal runoff and Indonesian throughflow in the tropical Indian Ocean. *Geophysical Research Letters*, *33*, L22609. <https://doi.org/10.1029/2006GL027573>
- Sherin, R., Durand, F., Gopalakrishna, V., Anuvinda, S., Chaitanya, A., Bourdallé-Badie, R., & Papa, F. (2018). Signature of Indian Ocean Dipole on the western boundary current of the Bay of Bengal revealed from 27 years of repeated in situ observations. *Deep-Sea Research, Part I*, *136*, 91–106. <https://doi.org/10.1016/j.dsr.2018.04.002>
- Shetye, S. R., Gouveia, A. D., Shankar, D., Shenoi, S. S. C., Vinayachandran, P. N., Sundar, D., et al. (1996). Hydrography and circulation in the western Bay of Bengal during the northeast monsoon. *Journal of Geophysical Research*, *101*(C6), 14011–14025. <https://doi.org/10.1029/95JC0330710.1029/95jc03307>
- Sprintall, J., & Tomczak, M. (1992). Evidence of the barrier layer in the surface layer of the tropics. *Journal of Geophysical Research*, *97*(C5), 7305. <https://doi.org/10.1029/92JC00407>
- Sree Lekha, J., Buckley, J. M., Tandon, A., & Sengupta, D. (2018). Subseasonal dispersal of freshwater in the northern Bay of Bengal in the 2013 summer monsoon season. *Journal of Geophysical Research: Oceans*, *123*, 6330–6348. <https://doi.org/10.1029/2018JC014181>
- Stuecker, M., Timmermann, A., Jin, F., Chikamoto, Y., Zhang, W., Wittenberg, A., et al. (2017). Revisiting ENSO/Indian Ocean Dipole phase relationships. *Geophysical Research Letters*, *44*, 2481–2492. <https://doi.org/10.1002/2016GL072308>
- Subrahmanyam, B., Murty, V., & Heffner, D. (2011). Sea surface salinity variability in the tropical Indian Ocean. *Remote Sensing of Environment*, *115*, 944–956. <https://doi.org/10.1016/j.rse.2010.12.004>
- Subrahmanyam, B., Trott, C., & Murty, V. (2018). Detection of Intraseasonal Oscillations in SMAP salinity in the Bay of Bengal. *Geophysical Research Letters*, *45*, 7057–7065. <https://doi.org/10.1029/2018GL078662>
- Suneel, V., Alex, M., Thomas, P., Gurumoorthi, K., Rao, V., Hari Krishnan, S., et al. (2020). Impact of remote equatorial winds and local mesoscale eddies on the existence of “River in the Sea” along the East Coast of India Inferred from Satellite SMAP. *Journal of Geophysical Research: Oceans*, *125*, e2020JC016866. <https://doi.org/10.1029/2020jc016866>
- Thadathil, P., Muraleedharan, P., Rao, R., Somayajulu, Y. K., Reddy, G. V., & Revichandran, C. (2007). Observed seasonal variability of barrier layer in the Bay of Bengal. *Journal of Geophysical Research*, *112*, C02009. <https://doi.org/10.1029/2006JC003651>
- Thadathil, P., Suresh, I., Gautham, S., Prasanna Kumar, S., Lengaigne, M., Rao, R. R., et al. (2016). Surface layer temperature inversion in the Bay of Bengal: Main characteristics and related mechanisms. *Journal of Geophysical Research: Oceans*, *121*, 5682–5696. <https://doi.org/10.1002/2016JC011674>
- Thompson, B., Gnanaseelan, C., & Salvekar, P. S. (2006). Variability in the Indian Ocean circulation and salinity and its impact on SST anomalies during dipole events. *Journal of Marine Research*, *64*, 853–880. <https://doi.org/10.1357/00224006779698350>
- Trott, C., Subrahmanyam, B., Murty, V., & Shriver, J. (2019). Large-scale fresh and salt water exchanges in the Indian Ocean. *Journal of Geophysical Research: Oceans*, *124*, 6252–6269. <https://doi.org/10.1029/2019JC015361>
- Vinayachandran, P., Murty, V., & Ramesh Babu, V. (2002). Observations of barrier layer formation in the Bay of Bengal during summer monsoon. *Journal of Geophysical Research*, *107*(C12), 8018–8021. <https://doi.org/10.1029/2001JC000831>
- Vinayachandran, P., & Nanjundiah, R. (2009). Indian Ocean sea surface salinity variations in a coupled model. *Climate Dynamics*, *33*, 245–263. <https://doi.org/10.1007/s00382-008-0511-6>
- Webster, P., Moore, A., Loschnigg, J., & Leben, R. (1999). Coupled ocean-atmosphere dynamics in the Indian Ocean during 1997–98. *Nature*, *401*(6751), 356–360. <https://doi.org/10.1038/43848>
- Wentz, F., Scott, J., Hoffman, R., Leidner, M., & Atlas, R. (2015). *Remote sensing systems Cross-Calibrated Multi-Platform (CCMP) 6-hourly ocean vector wind analysis product on 0.25 deg grid, Version 2.0*. Santa Rosa: Remote Sensing Systems. Retrieved from www.remss.com/measurements/ccmp
- Yu, L., & Weller, R. (2007). Objectively analyzed air-sea heat fluxes for the global oce-free oceans (1981–2005). *Bulletin of the American Meteorological Society*, *88*, 527–540. <https://doi.org/10.1175/bams-88-4-527>
- Zhang, L., Du, Y., & Cai, W. (2018). Low-frequency variability and the unusual Indian Ocean Dipole events in 2015 and 2016. *Geophysical Research Letters*, *45*, 1040–1048. <https://doi.org/10.1002/2017GL076003>
- Zhou, L., & Murtugudde, R. (2014). Impact of northward-propagating intraseasonal variability on the onset of Indian summer monsoon. *Journal of Climate*, *27*(1), 126–139. <https://doi.org/10.1175/JCLI-D-13-00214.1>
- Zuo, H., Balmaseda, M., Tietsche, S., Mogensen, K., & Mayer, M. (2019). The ECMWF operational ensemble reanalysis-analysis system for ocean and sea ice: A description of the system and assessment. *Ocean Science*, *15*(3), 779–808. <https://doi.org/10.5194/os-15-779-2019>